SMR rapport

A WATER QUALITY MODEL FOR A TROPICAL ESTUARY IN COSTA RICA

SMR-rapport 33/99

UNIVERSITETET I BERGEN
SENTER FOR MILJØ- OG RESSURSSTUDIER

ISSN 0803-7132

SENTER FOR MILJØ- OG RESSURSSTUDIER
Universitetet i Bergen

Høyteknologisenteret, N-5020 Bergen, Norway Tel.: +47 55 58 42 40 Fax.: +47 55 58 96 87

Report nr.: 33/99
Distibution: OPEN

Title
A water quality model for a tropical estuary in Costa Rica

Date: 01.12.99
Pages: 50

Author(s)
Rune Rosland

Project manager
Ulf Lie

Contractors
Research Council of Norway
University of Bergen

Contractors' ref.

Abstract
A model for water quality and circulation is developed and implemented for the fjord-like estuary Golfo Dulce, which is located at the southern pacific coast of Costa Rica. The model is based on existing models for water circulation, primary production and recycling processes. The prognostic state variables are water circulation, hydrography, oxygen, phytoplankton biomass, nutrients and dead organic and inorganic matter. The main forcing functions represent wind, freshwater runoff, tides, boundary conditions (hydrography, nutrients and organic material) and solar radiation at the sea surface. The report presents some preliminary model simulations of the physical and biological system of Golfo Dulce. The simulations indicate that freshwater, tides and bottom topography are all influential on the circulation patterns in the gulf, while the Coriolis effect seems rather weak. Advection of coastal water may be important for the phytoplankton production in the gulf. Effects from changes in river nutrients seem to be moderate within the ranges tested here. The simulations indicate that inorganic substances in river water may have pronounced effects on light regimes and phytoplankton production in the gulf. However, comparisons of predicted and observed nutrient concentrations and primary production indicate a need for parameter adjustments and/or modifications of the biological model.

Keywords
Golfo Dulce, water quality model, circulation, hydrography

Project manager

Administration

Table of contents

Introduction

The tropical estuary Golfo Dulce is located at the southern Pacific coast of Costa Rica (Figure 1). Unlike other estuaries in the region, the bottom topography of Golfo Dulce resembles that of a temperate fjord, with a deep inner basin separated from the coastal water by a shallower sill. Although human exploitation in Golfo Dulce is moderate, the later years activities in forestry, agriculture and construction have induced changes in area (Wolff et al. 1996). Since the mid seventies, large parts of the low land of Osa peninsula has been deforested for agriculture (Sader & Joyce 1988; Cortés 1990), and rivers in the Osa mountains have been mined for gold (Berrangé 1989). Tourism industry is growing, and agro-industrial projects, such as wood-chips mills, fish farming, shrimp and oyster cultures are suggested in the area. The growing industrial activities have lead to a growth in the local human population in Golfo Dulce. It is expected that the human activities already are, and will continue with a growing strength, to influence the marine and terrestrial ecosystem of Golfo Dulce. Impacts from industry, agriculture, forestry, tourism and households may increase erosion, sedimentation and input of organic matter, nutrients and chemicals to the marine ecosystem of Golfo Dulce.

Although Golfo Dulce is an atypical tropical estuary, there seem to be relatively few studies on Golfo Dulce compared to other estuaries in the area. Ecosystems are complex systems with many different and interacting processes. Natural large-scale ecosystems normally exclude the possibility to perform controlled experiments, and numerical models have therefore turned out to be useful in the study of these systems (Stephens & Krebs 1986; Jørgensen 1994; Visser & Kamp-Nielsen 1996). Numerical models provide an opportunity to perform scientific experiments on and to make predictions about complex natural systems. Today's computer technology makes it possible to develop operational models, with sufficient complexity, to make realistic simulations of some parts of natural systems. Amongst these are the coupled models for water circulation and marine phytoplankton production, e. g. Aksnes et al. (1995) and Skogen et al. (1996), used to study eutrophication processes. Since many of the variables in these models are also relevant parameters for water quality, these models are also interesting as tools for water quality studies.

The aim of this project was to develop a numerical model to study the influences from natural (wind, tides, freshwater, oceanic) and human processes (fertilisation, non-natural pollutants, and erosion) on the marine system in Golfo Dulce. The coupled model for water quality is based on a three-dimensional barocline circulation model (Blumberg & Mellor 1987; Berntsen et al. 1996, 1997) and a biological model for primary production (Aksnes et al. 1994, 1995) and nutrient recycling (Savchuk and Wulff 1996). The model is driven by external forcing functions at the land, air, ocean and bottom boundaries. The quality of the forcing functions will clearly have a strong influence on the model output. The lack of empirical data from Golfo Dulce makes it an interesting study site. Lack of field data, on the other hand, also makes it difficult to create realistic forcing functions and to verify the predictions from the model. Therefore, a mix of data from large-scale databases and available data from the area constituted the base of the forcing functions.

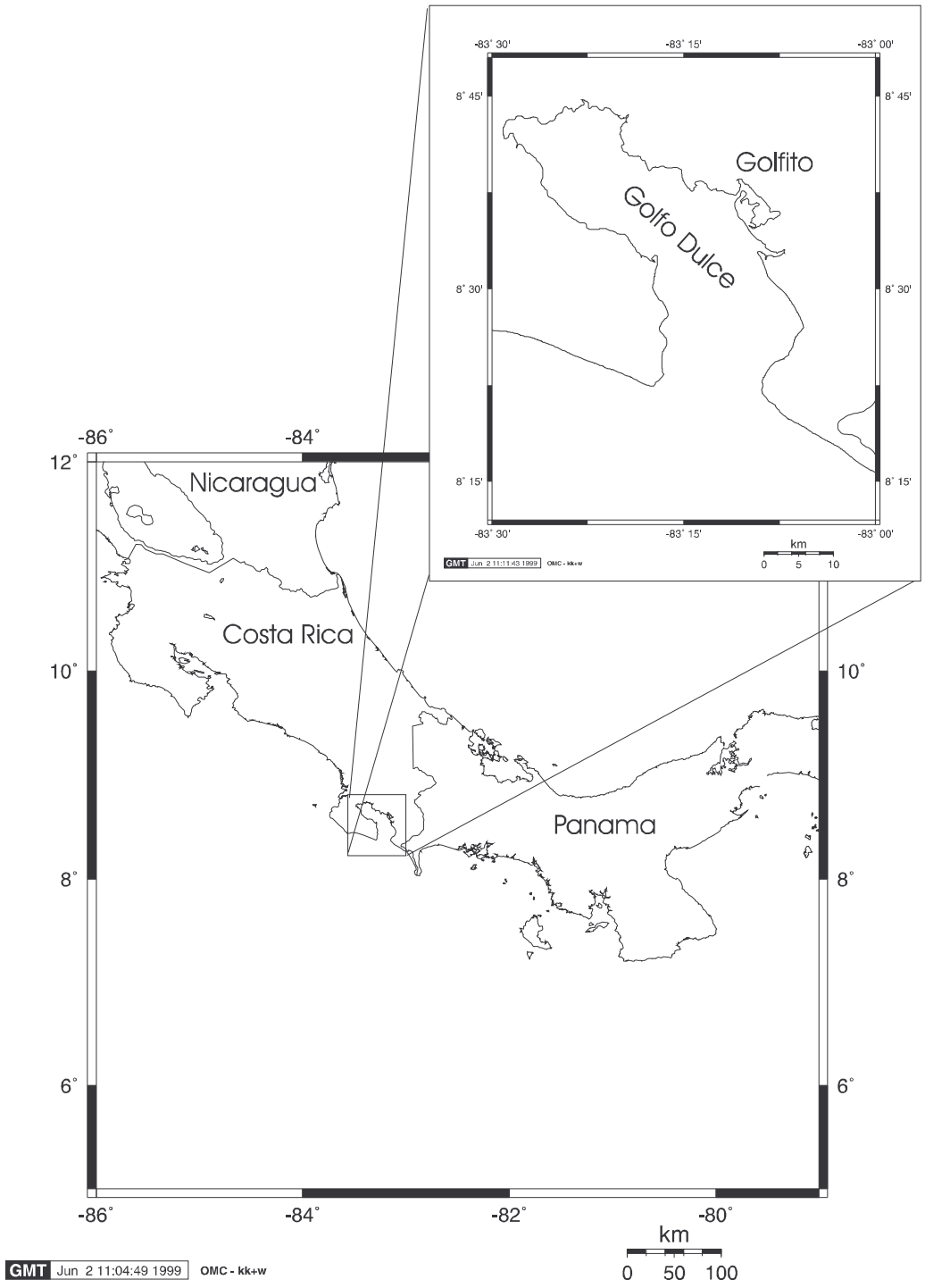

FIGURE 1. Geographic maps of Costa Rica and Golfo Dulce

This report documents the results obtained during the "water quality modelling project" in Golfo Dulce in 1997 and 1998. Presented are some preliminary model simulations of the marine system of Golfo Dulce. Although lack of proper field data reduces the realism of the model, it may still give interesting indications about the dominating processes in Golfo Dulce. However, a through evaluation and validation of the model have to wait until more field data are available from the area.

Characteristics of Golfo Dulce

Golfo Dulce is a tropical estuary located at the southern pacific coast of Costa Rica (Figure 1). The gulf is about 10-15 km wide and 50 km long with a surface area about 750 km^2. The small surface-volume ratio and the shallow sill at the mouth make Golfo Dulce resembling a typical high latitude temperate fjord (Richards et al. 1971; Hebbeln et al. 1996). The gulf can be divided into an inner and an outer basin. The inner basin is flat and deep, with steep slopes and a maximum depth about 215 m. The outer basin is shallower, with a sill at about 60 m separating the gulf basin from adjacent coastal water (Hebbeln et al. 1996; Wolff et al. 1996). Anoxic conditions has been reported in the inner basin, but it is not established whether these conditions occur periodically or permanently (Richards et al. 1971; Brenes & Léon 1988; Thamdrup et al. 1996).

The gulf may further be divided into two vertical zones. The upper layer is stratified, and reaches down to about 50-60 m. It has diluted salinity (< 34 ‰) and temperatures ranging from 19-30 °C. The deeper layer is more homogeneous, with salinity around 34.8 ‰ and a minimum temperature around 15.4 °C (Brenes & Léon 1988; Thamdrup et al. 1996).

Tidal amplitudes in the inner basin range between 2-4 m (Quirós 1989). Tidal currents are strong across the sill, but they presumably attenuate rapidly towards the inner basin, which is characterised by sluggish currents and minimal water transport (Quirós 1989, 1990). The climate is hot and humid, with rain all year around. Precipitation exceeds evaporation at least 8 months of the year (Herrera 1985). The dry season, lasting from January to March, has monthly precipitation on average less than 100 mm (Herrera 1985). The wet season, lasting from April to December, has monthly precipitation on average above 500 mm, usually with a maximum in October (Herrera 1985). In spite of heavy precipitation, the river driven water transport is assumed to be small compared to the tidal transport, and freshwater is assumed have less influence on the water circulation in Golfo Dulce (Quirós 1989). Seasonal rain, however, may influence surface salinity and temperatures (Yukihira 1991). Surface flushing is limited to the upper 0-5 meters of the gulf. The exchange of deep water is suggested to be a slow process that most likely is caused by intrusion of subsurface coastal water (Richards et al. 1971).

The model

The water quality model (Figure 2) is based on two separate and independent models:

- a *physical model* for hydrography and water circulation
- a *biological* model for chemical and biological dynamics

The physical model constitutes the skeleton/frame of the coupled model, and the biological model may be considered as an additional module to the physical model. The biological model depends on input of water transport and temperature from the physical model (Figure 2).

Hydrography and water circulation

The physical model is developed by Berntsen et al. (1996). It is a modified version of the three-dimensional coastal ocean circulation model, better known as the *Princeton Ocean Model* (POM), developed by Blumberg & Mellor (1987). The major modifications from POM are found in the advection terms, the implicit time calculations and the splitting of time into 2- and 3-dimensional calculations. The prognostic variables of the physical model include:

- three components of water velocity
- temperature
- salinity
- surface water elevation
- turbulence (kinetic and macro scale)

The basic equations are: the momentum equations, the continuity equations, conservation equations for temperature and salinity and a turbulence closure model for the turbulent kinetic energy (Mellor & Yamada 1982). The governing equations and the variables of the physical model are listed in Tables 1 and 2, respectively. For a more detailed description of the physical model see Blumberg & Mellor (1987) and Berntsen et al. (1996).

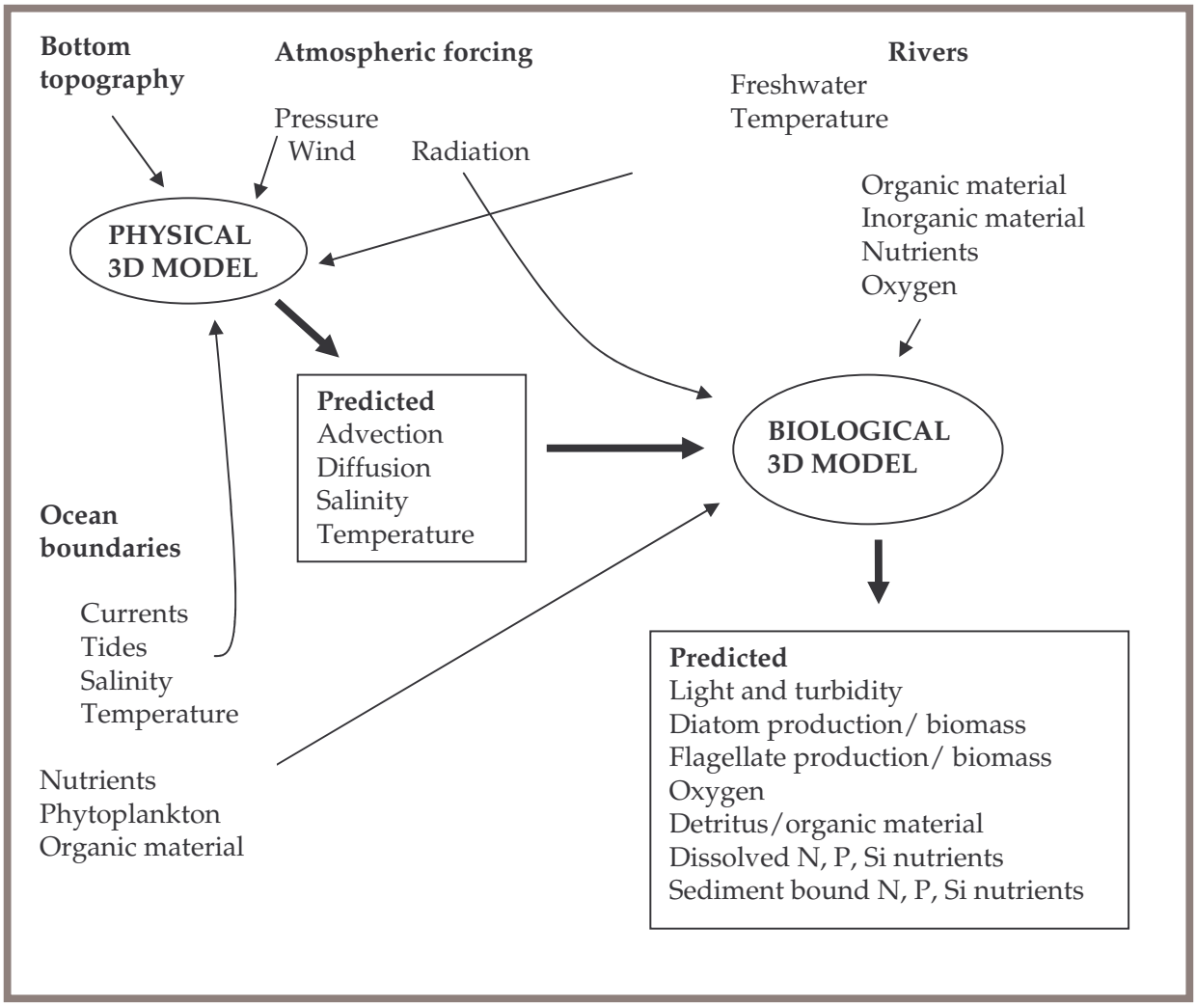

FIGURE 2. A conceptual map of the coupled physical-chemical-biological water quality model

Table 1. The main equations of the physical model.

EQUATION	DESCRIPTION	PROCESS FORMULATION
P1	Continuity equation	$\nabla \cdot \vec{U} + \frac{\partial W}{\partial z} = 0$
P2	Momentum equation for U	$\frac{\partial U}{\partial t} + \vec{U} \cdot \nabla U + W \cdot \frac{\partial U}{\partial z} - fV = -\frac{1}{\rho_0} \cdot \frac{\partial P}{\partial x} + \frac{\partial}{\partial z}\left(K_M \cdot \frac{\partial U}{\partial z} \right) + F_x$
P3	Momentum equation for V	$\frac{\partial V}{\partial t} + \vec{U} \cdot \nabla V + W \cdot \frac{\partial V}{\partial z} + fU = -\frac{1}{\rho_0} \cdot \frac{\partial P}{\partial y} + \frac{\partial}{\partial z}\left(K_M \cdot \frac{\partial V}{\partial z} \right) + F_y$
P4	Pressure	$P = g \cdot \rho_0 \cdot \eta + g \cdot \int_z^0 \rho(\dot{z}) d\dot{z}$
P6	Conservation equation for salinity	$\frac{\partial S}{\partial t} + \vec{U} \cdot \nabla S + W \cdot \frac{\partial S}{\partial z} = \frac{\partial}{\partial z}\left(K_H \cdot \frac{\partial S}{\partial z} \right)$
P7	Conservation equation for temperature	$\frac{\partial T}{\partial t} + \vec{U} \cdot \nabla T + W \cdot \frac{\partial T}{\partial z} = \frac{\partial}{\partial z}\left(K_H \cdot \frac{\partial T}{\partial z} \right)$
P8	Conservation equation for chemical and biological variables	$\frac{\partial Bio}{\partial t} + \vec{U} \cdot \nabla Bio + W \cdot \frac{\partial Bio}{\partial z} = \frac{\partial}{\partial z}\left(K_M \cdot \frac{\partial Bio}{\partial z} \right) - \frac{\partial}{\partial x}\left(A_H \cdot \frac{\partial Bio}{\partial x} \right) - \frac{\partial}{\partial y}\left(A_H \cdot \frac{\partial Bio}{\partial y} \right)$

Table 2. The variables of the physical model

SYMBOL	DESCRIPTION	UNIT
$\vec{U} = (U, V)$	Horizontal velocities in x- and y-direction respectively	m s^{-1}
$\vec{U}_b = (U_b, V_b)$	Horizontal velocity at the bottom	m s^{-1}
η	Surface elevation	m
ρ	Density	kg m^{-3}
ρ_0	Reference density	kg m^{-3}
A_H	Horizontal eddy diffusivity	m^2 s^{-1}
A_M	Horizontal eddy viscosity	m^2 s^{-1}
D	Bottom dynamic depth	m
F_x, F_y	Horizontal components of diffusion	
f	The coriolis parameter	s^{-1}
g	Gravity	m s^{-2}
H	Bottom static depth	m
K_H	Vertical eddy diffusivity	m^2 s^{-1}
K_M	Vertical eddy viscosity	m^2 s^{-1}
P	Pressure	N m^{-2}
S	Salinity	g cm^{-3}
T	Temperature	°C
W	Vertical velocity in z-direction	m s^{-1}

Nutrient recycling and primary production

The biological model is a fusion of two models for phytoplankton growth (Aksnes et al. 1995; Savchuk & Wulff 1996) and nutrient recycling (Savchuk & Wulff 1996). The biological model (Figure 3) simulates the cycling of nutrients between dead organic substances, dissolved inorganic molecules and primary producers. In addition, the model keeps track of oxygen consumed and produced by different processes. The model includes state variables of sediment bound nutrients. State variables and the main state equations of the biological model are listed in Table 3. Parameters and variables of the sub-processes are listed in Tables 4 and 5, respectively. A detailed description of the biological model is presented in the following.

Table 3. The main process equations of the biological model. The equations for sub-processes are found in the text.

EQUATION	STATE VARIABLE	PROCESS EQUATION
B1	Nitrate	$\frac{\partial Nit}{dt} = nitrA + sedoN - phoN - denitr$
B2	Ammonium	$\frac{\partial Amm}{dt} = dmir(A) + exc(A) + sedoA - phoA - nitrA$
B3	Phosphor	$\frac{\partial Pho}{dt} = dmir(P) + exc(P) + smir(P) - phoP$
B4	Silicon	$\frac{\partial Sil}{dt} = dmir(Si) + smir(Si) - phoSi$
B5	Oxygen	$\frac{\partial Oxy}{dt} = phoO + denitrO - mirO - nitrO - sedres$
B6	Detritus nitrogen	$\frac{\partial DetN}{dt} = grd(N) - dmir(A) + sidet_{in}(N) - sidet_{out}(N)$
B7	Detritus phosphor	$\frac{\partial DetP}{dt} = grd(P) - dmir(P) + sidet_{in}(P) - sidet_{out}(P)$
B8	Detritus silicon	$\frac{\partial DetS}{dt} = grd(S) - dmir(Si) + sidet_{in}(P) - sidet_{out}(P)$
B9	Diatom biomass	$\frac{\partial Dia}{dt} = Dia \cdot (g_{dia} - pex - \mu) + sidia_{in} - sidia_{out}$
B10	Flagellate biomass	$\frac{\partial Fla}{dt} = Fla \cdot (g_{fla} - pex - \mu)$
B11	Sediment nitrogen	$\frac{\partial SedN}{\partial t} = sidia + sidet(N) - smir(A) + bur(N)$
B12	Sediment phosphorous	$\frac{\partial SedP}{\partial t} = r_{diaP} \cdot sidia + sidet(P) - smir(P) + seqP - bur(P)$
B13	Sediment silicon	$\frac{\partial SedSi}{\partial t} = r_{diaSi} \cdot sidia + sidet(Si) - smir(Si)$

Table 4. Parameters in the biological model

SYMBOL	DESCRIPTION	UNIT	VALUE
α_{dia}	diatom growth coefficient at 0 °C	s^{-1}	$1.5*10^{-5}$
α_{dmir}	detritus mineralization rate	d^{-1}	0.002
α_{fla}	flagellate growth coefficient at 0 °C	s^{-1}	$1.0*10^{-5}$
α_{nitrif}	nitrification coefficient	d^{-1}	0.01
α_{pex}	metabolic loss/waste rate of phytoplankton at 0 °C	s^{-1}	$8.1*10^{-7}$
α_{sidet}	detritus sinking rate	m d^{-1}	1.5
α_{smir}	mineralization of sediment nitrogen	d^{-1}	0.001
α_{zoo}	heterotropic growth efficiency koeff.	m d^{-1}	
β_{dia}	temperature coefficient on diatom growth	C^{-1}	0.063
β_{dmir}	temperature coefficient in detritus mineralization	C^{-1}	0.15
β_{nitrif}	temperature coefficient on nitrification	C^{-1}	0.15
β_{pex}	temperature coeff. on phytopl. metabolic loss/waste rate	C^{-1}	0.07
β_{sidet}	temperature coefficient in detritus sinking	C^{-1}	0.1
β_{smir}	temperature coeff. on sediment nitrogen mineralization	C^{-1}	0.03
β_{zoo}	temperature coefficient on heterotroph growth eff.	C^{-1}	
$\varepsilon_{denitrO}$	denitrification exponent	-	6.0
ε_{ϕ}	exponential coeff. on ammonium/nitrate preference	-	6.0
k_{aer}	coeff. on oxygen dependence on phosphate processes	-	7.5
k_{ana}	coeff. for oxygen dependence on phosphate processes	gO_2 m^{-3}	100
k_{as}	coefficient in sediment red-ox potential	-	5.0
k_{AtoS}	Frac. of mineralized sediment amm. becoming sediment particles	-	0.5
k_{bs}	coefficient in sediment red-ox potential	$(gO_2\ m^{-3})^{-1}$	0.9
k_{bur}	burial rate of nutrients in the sediments	m d^{-1}	$1.0*10^{-5}$
k_{cs}	coefficient in sediment red-ox potential	-	0.004
k_{denitr}	denitrification coefficient	d^{-1}	0.5
$k_{denitrN}$	half saturation coefficient for denitrification	mgN m^{-3}	14.0
$k_{denitrO}$	oxygen equivalents for denitrification	gO_2 mgN^{-1}	0.003
k_{detO}	oxygen equivalents for mineralization of detritus	gO_2 mgN^{-1}	0.015
k_{diaI}	diatom light affinity	$microE^{-1}$ m^2	$3.6*10^{-6}$
k_{diaN}	diatom nitrogen affinity	mgN^{-1} m^3 s^{-1}	$1.2*10^{-6}$
k_{diaP}	diatom phosphorous affinity	mgN^{-1} m^3 s^{-1}	$8.7*10^{-6}$
k_{diaSi}	diatom silicon affinity	mgN^{-1} m^3 s^{-1}	$8.9*10^{-7}$
k_{ϕ}	ammonium threshold for ammonium/nitrate preference	mg NH_4 m^{-3}	14.0
k_{flaI}	flagellate light affinity	$microE^{-1}$ m^2	$1.1*10^{-6}$
k_{flaN}	flagellate nitrogen affinity	mgN^{-1} m^3 s^{-1}	$7.4*10^{-6}$
k_{flaP}	flagellate phosphorous affinity	mgN^{-1} m^3 s^{-1}	$1.1*10^{-6}$
k_{nitrI}	photo inhibition coefficient	m^2 W^{-1}	0.1
k_{nitrO}	oxygen equivalents for nitrification	gO_2 mgN^{-1}	0.0046
k_{ox}	coefficient in sediment red-ox potential	-	0.6
$k_{oxdenitr}$	oxygen concentration where denitrification starts	gO_2 m^{-3}	0.72
k_{oxnitr}	half saturation constant for anoxic inhibition of nitrification	gO_2 m^{-3}	0.0143
k_{pho}	oxygen equivalents for primary production	gO_2 mgN^{-1}	0.02
k_{sidia}	shape factor for diatom sink function	mgN m^{-2} s^{-1}	$8.78*10^{-4}$
$k_{sidiaMax}$	maximum diatom sinking rate	m s^{-1}	$3.47*10^{-5}$
$k_{sidiaMin}$	minimum diatom sinking rate	m s^{-1}	$3.47*10^{-6}$
$k_{silsink}$	silicate concentration threshold for diatom sinking	mgSi m^{-3}	28.09
k_{zass}	heterotroph assimilation efficiency		
k_{zoores}	oxygen equivalents of heterotroph respiration		
μ	phytoplankton mortality rate	s^{-1}	$1.6*10^{-6}$
r_{diaP}	phosphor/nitrate ratio in diatom cells	mgP mgN^{-1}	0.138
r_{diaSi}	silicate/nitrate ratio in diatom cells	mgS mgN^{-1}	1.750
r_{flaP}	phosphor/nitrate ratio in flagellate cells	mgP mgN^{-1}	0.138

Table 5. Functions and variables in the biological model

SYMBOL	DESCRIPTION	UNIT
bur(..)	burial of nutrients (N,P) into the sediments	mg m^{-2} d^{-1}
denitr	nitrate converted to molecular nitrogen in denitrification	mg N m^{-3} d^{-1}
denitrO	oxygen produced in denitrification of nitrate	g O_2 m^{-3} d^{-1}
dmir(..)	mineralization of detritus (*Amm, Pho, Sil*)	mg m^{-3} d^{-1}
exc(..)	exctetion from phytoplankt. and heterotrophs (*Amm, Pho*)	mg P m^{-3} d^{-1}
ϕ	fraction between nitrate/ammonium preference	-
g_{dia}	limited diatom growth rate	d^{-1}
g_{fla}	limited flagellate growth rate	d^{-1}
g_{max}	unlimited phytoplankton growth rate	d^{-1}
grd(..)	grazed phytopl. and detritus entering detritus (N,P,Si) pools	
I_w	light intensity in Watt	W m^{-2}
mirO	oxygen consumed in mineralization of detritus	g O_2 m^{-3} d^{-1}
N	available nitrogen nutrients (balanced ammonium+nitrate conc.)	mg N m^{-3} d^{-1}
ν_{dnitr}	nitrate dependence on denitrification	mg N m^{-3}
nitrA	ammonium converted to nitrate in nitrification	mg m^{-3} d^{-1}
nitrO	oxygen consumed in nitrification of ammonium	g O_2 m^{-3} d^{-1}
oxdenitr	oxygen dependence of denitrification	mg N m^{-3}
oxnitr	oxygen dependence of nitrification	gO_2 m^{-3}
pex	phytoplankton metabolic losses/wastes	mg N d^{-1}
phoA	ammonium consumed in primary production	mg N m^{-3} d^{-1}
phoN	nitrate consumed in primary production	mg N m^{-3} d^{-1}
phoO	oxygen produced in primary production	g O_2 m^{-3} d^{-1}
phoP	phosphorous consumed in primary production	mg P m^{-3} d^{-1}
phoSi	silicate consumed in primary production	mg S m^{-3} d^{-1}
q_{PtoS}	sediment oxygen conditions for phosphorous processes	
q_{SAtoW}	sediment red-ox condition for nitrogen processes	-
q_{SNtoW}	red-ox condition in the upper sediment	-
sedoA	ammonification of nitrogen mineralized from sediments	mg N m^{-3} d^{-1}
sedoN	nitrate released from sediments via ammonium	mg N m^{-3} d^{-1}
sedres	respiration by sediment processes	g O_2 m^{-3} d^{-1}
seqP	fraction of mineralized phosphorous returning to sediment	
sidet(..)	detritus sinking function (N,P,S - pool)	mg m^{-3} d^{-1}
sidia	sinking rate of diatoms	mg N m^{-3} d^{-1}
smir(..)	mineralization of sediments (*Amm, Pho, Sil*)	mg m^{-3} d^{-1}
T	water temperature	degrees C
Z_b	depth interval in depth cell above bottom	m
zex	heterotroph excretion rate	
zgreff	heterotroph growth efficiency	
zoores	oxygen consumed in heterotroph respiration	

The amount and distribution of nutrients in the ocean may be influenced by many factors. This model includes:

- photosynthetic production and losses
- nitrification and denitrification
- mineralisation of detritus particles
- sedimentation of inorganic and organic material
- mineralisation of sediment bound nutrients
- diffusion and advection (see Eq. P8 in Table 1)

The state variables in the biological model represent different pools of nutrients and seawater oxygen concentrations:

- free inorganic nutrients (nitrate, ammonium, phosphate, silicate)
- nutrients (nitrogen, phosphorous, silicon) bound in dead organic matter
- nutrients (nitrogen, phosphorous, silicon) bound in diatom and flagellate phytoplankton
- nutrient (nitrogen, phosphorous, silicon) bound in sediments
- oxygen in the water

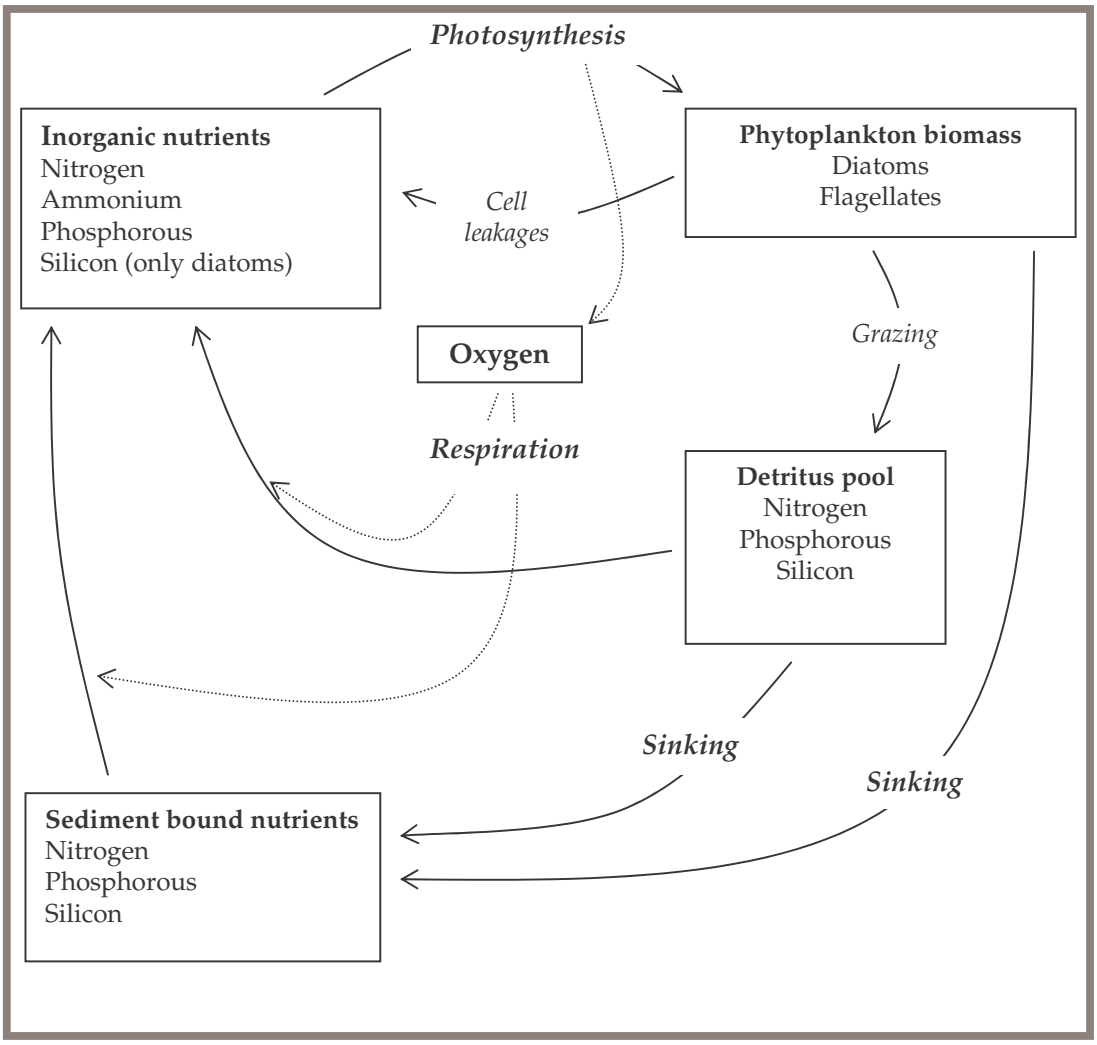

FIGURE 3. Conceptual map of the biological module of the water quality model

The model includes phytoplankton dynamics only, and the top-down regulation of phytoplankton production is simply represented by a grazing parameter. This model concept was chosen because higher trophical dynamics are far more complex, involving age-structured populations of individuals with behavioural abilities. Presently there are no models of these complex dynamics that would do better, in terms of representing a top-down regulation on modelled primary production, than a simple grazing parameter.

Water bound processes

The circulation model (Eq. P8 in Table 1) calculates the turbulent diffusion and advective processes determining transports of nutrients, phytoplankton, detritus and oxygen. The main state equations of the biological model are listed in Table 3. Turbulent diffusion and advection act on all the biological state variables, but the terms were left out from the equations in Table 1 in order to simplify reading. Biological parameters and variables are listed in Tables 3-5.

Nitrate (representing all dissolved inorganic nitrogen compounds except ammonium)

Nitrate concentration (*Nit* in Eq. B1, Table 3) increases with nitrate inputs from nitrification of ammonium in water (*nitrA*) and in sediments (*sedoN*). The concentration decreases with losses from denitrification (*denitr*) and photosynthetic production (*phoN*). Nitrification rate (ammonium is oxidised to nitrate) is a function of ammonium concentration (*Amm*):

$$nitrA = \frac{oxnitr}{1 + k_{nitrI} \cdot I_w} \cdot \left[\alpha_{nitrif} \cdot \exp(\beta_{nitrif} \cdot T) \right] \cdot Amm \qquad \text{B1.1}$$

The function accounts for light (I_w) inhibition and oxygen inhibition (*oxnitr*) at low oxygen concentrations (Kaplan 1983; Henriksen & Kemp 1988; Enoksen et al. 1990). The temperature dependency is calculated from an exponential function of water temperature (T). (see Table 4 for the coefficients α_{nitrif}, β_{nitrit}, k_{nitrI}). Inhibition from oxygen (*oxnitr*) is calculated as a switch function (see Table 4 for k_{oxnitr}):

$$oxnitr = \begin{cases} 0 & \text{at } Oxy \le 0 \\ \dfrac{Oxy}{k_{oxnitr} + Oxy} & \text{at } Oxy > 0 \end{cases} \qquad \text{B1.1.1}$$

Since negative oxygen concentration is allowed (representing anoxic conditions) the function is zero by definition for negative values of oxygen concentrations.

Denitrification (reduction of nitrate to molecular nitrogen) occurs at low oxygen concentrations. The formulation used here generates a sharp initialisation of denitrification (*denitr*) at low oxygen concentrations (see Table 4 for k_{dnitr}):

$$denitr = \begin{cases} 0 & \text{at } Nit \le 0 \\ k_{denitr} \cdot oxdenitr \cdot \nu_{denitr} \cdot Nit & \text{at } Nit > 0 \end{cases} \qquad \text{B1.2}$$

Oxygen dependency is given by the function:

$$oxdenitr = \frac{1}{1+\left(\frac{Oxy}{k_{oxdenitr}}\right)^{\varepsilon_{denitrO}}} \qquad \text{B1.2.1}$$

See Table 4 for values of $\varepsilon_{denitrO}$ and $k_{denitrN}$. The nitrate dependency is given by a half-saturation function:

$$v_{denitr} = \frac{Nit}{k_{denitrN} + Nit} \qquad \text{B1.2.2}$$

Nitrate consumed in primary production (*phoN*):

$$phoN = \frac{\left(g_{dia} \cdot Dia + g_{fla} \cdot Fla\right) \cdot \phi}{Amm + \phi \cdot Nit} \cdot Nit \qquad \text{B1.3}$$

Here g_{dia} and g_{fla} represent diatom and flagellate growth rate, respectively. The variable ϕ defines the relative preference between nitrate (*Nit*) and ammonium (*Amm*), and is a function of ammonium concentration (see Table 4 for k_ϕ and ε_ϕ.):

$$\phi = \frac{1}{1+\left(\frac{Amm}{k_\phi}\right)^{\varepsilon_\phi}} \qquad \text{B1.3.1}$$

Ammonium

Ammonium concentration (*Amm*, Eq. B2, Table 3) increases with inputs from excretion (*exc(A)*) and mineralisation of detritus (*dmir(A)*) and sediment bound nitrogen compounds (*sedo(A)*). The concentration decreases with losses to primary production (*pho(A)*) and nitrification (*nitrA*).

Photosynthetic consumption of ammonium is calculated as:

$$phoA = \frac{g_{dia} \cdot Dia + g_{fla} \cdot Fla}{Amm + \phi \cdot N} \cdot Amm \qquad \text{B2.1}$$

Here g_{dia} and g_{fla} represent diatom and flagellate growth rates, and ϕ the preference between nitrogen sources (Eq. B1.3.1).

Mineralisation of detritus to ammonia (*dmir(A)*) is a function of temperature (*T*) and detritus concentration (*DetN*) (see Table 4 for α_{dmir} and β_{dmir}):

$$dmir(A) = \alpha_{dmir} \cdot \exp\left(\beta_{dmir} \cdot T\right) \cdot DetN \qquad \text{B2.2}$$

Excretion of ammonium (*exc(A)*) is given in Eq. B10.3 and release of ammonium from sediments (*sedoA*) in Eq. B11.3.

Phosphate (representing all dissolved inorganic phosphorous compounds)
Phosphate concentration (*Pho*, Eq. B3, Table 3) increases with inputs from excretion (*exc(P)*) and mineralisation of detritus (*dmir(P)*) and sediment bound phosphorous compounds (s*mir(P)*). Phosphate concentration decreases with losses to photosynthetic production (*phoP*).

Phosphate consumed in photosynthetic production is a function of phytoplankton growth:

$$phoP = r_{diaP} \cdot g_{dia} \cdot Dia + r_{flaP} \cdot g_{fla} \cdot Fla \qquad \text{B3.1}$$

The coefficients r_{diaP} and r_{flaP} (Table 4) define the *P:N* ratio in diatoms and flagellates, and the variables g_{dia} and g_{fla} represent growth in the two phytoplankton groups.

Detritus mineralisation (*dmir(P)*) is calculated by an equation analogous to Eq. B2.2, but with phosphorous detritus (*DetP*) as functional value. Excretion of phosphorous (*exc(P)*) is calculated in Eq. B10.4.

Silicate (representing all dissolved inorganic silicon compounds)
Silicate concentration (*Sil*, Eq. B4, Table 3) increases with input from mineralisation of detritus (*dmir(Si)*) and sediment bound silicon (*dmir(Si)*). Concentration decreases with losses to photosynthetic production (*phoSi*).

Silicate consumed in photosynthetic production is a function of diatom growth rate:

$$phoSi = \left(r_{diaSi} \cdot g_{dia}\right) \cdot Dia \qquad \text{B4.1}$$

The coefficient r_{diaSi} (Table 4) define the *Si:N* ratio in a diatom cell. The variable g_{dia} is diatom growth rate.

Mineralisation of detritus (*dmir(Si)*) is calculated by an equation analogous to Eq. B2.2, but with detritus bound silicon (*DetSi*) as the functional value.

Oxygen
Oxygen concentration (*Oxy*, Eq. B5, Table 3) increases with inputs from photosynthetic production (*phoO*) and denitrification (*denitrO*). Oxygen decreases with losses to heterotroph respiration (*zoores*), mineralisation processes (*dmirO*), nitrification (*nitrO*) and oxygen consuming sediment processes (*sedres*).

Photosynthetic oxygen production is a function of phytoplankton growth (g_{dia} and g_{fla}):

$$phoO = k_{pho} \cdot \left(g_{dia} \cdot Dia + g_{fla} \cdot Fla\right) \qquad \text{B5.1}$$

Oxygen consumed in the ammonification of detritus is:

$$mirO = k_{detO} \cdot dmir(A) \qquad \text{B5.2}$$

Oxygen consumed in nitrification is:

$$nitrO = k_{nitrO} \cdot nitrA \qquad \text{B5.3}$$

Oxygen produced (*denitrO*) in the denitrification process is:

$$denitrO = k_{denitrO} \cdot denitr \qquad \text{B5.4}$$

Oxygen respired by heterotroph organisms grazing on phytoplankton and detritus is calculated from the amount of excreted ammonium (*exc(A)* in Eq. B10.3):

$$zoores = k_{zoores} \cdot exc(A) \qquad \text{B5.5}$$

The coefficients k_{pho}, k_{detO}, k_{nitrO}, $k_{denitrO}$ and k_{zoores} (Table 4) are oxygen equivalents of photosynthesis, ammonification, nitrification, denitrification and heterotroph respiration (Gundersen & Mountain 1973; Klump & Martens 1983). Sediment respiration processes (*sedres*) are calculated in Eq. B14.

Detritus

Detritus is divided into pools of nitrogen (*DetN*, Eq. B6), phosphorous (*DetP*, Eq. B7) and silicon (*DetSi*, Eq. B8). The pools are regulated by inputs from phytoplankton mortality (*grd(N,P,S)*) losses to mineralisation processes (*dmir(A,P,S)*). The sinking of detritus represents both a source and sink. Sinking rate (*sidet*), as exemplified for nitrogen detritus in Eq. B6.1, depends on temperature (see Table 4 for α_{sidet} and β_{sidet}):

$$sidet(N) = \alpha_{sidet} \cdot \exp(\beta_{sidet} \cdot T) \cdot DetN \qquad \text{B6.1}$$

The variable *DetN* in Eq. 6.1 represents detritus concentrations in depths above current depth for *in*sinking detritus ($sidet_{in}$ in Eqs B6-B8) and detritus concentrations in the current depth cell for *out*sinking detritus ($sidet_{out}$ in Eqs B6-B8).

Phytoplankton

Phytoplankton contains two categories: flagellates and diatoms. Diatoms require silicon for growth and are assumed to have higher affinities for light and nutrients than flagellates (Aksnes et al. 1994). As a consequence, diatoms will outgrow flagellates under all circumstances unless limited by silicon nutrients.

Diatom biomass (Eq. B9, Table 3) depends on growth rate (g_{dia}), excretion (*pex*), mortality (μ) and sinking ($sidia_{in}$ and $sidia_{out}$). Unlimited by light and nutrients, phytoplankton growth follows an exponential function of temperature (see Table 4 for α_{dia} and β_{dia}):

$$g_{\max} = \alpha_{dia} \cdot \exp(\beta_{dia} \cdot T) \qquad \text{B9.1}$$

Limitations from light and nutrients are calculated as half saturation functions:

$$X_{\lim} = X \cdot \left(\frac{g_{\max}}{k_X} + X \right)^{-1} \qquad \text{B9.2}$$

Temperature dependent half saturation (X_{lim}) is given by g_{max}/k_X, where X represents the limiting factor (light or nutrient). Phytoplankton affinities for light and nutrients (k_{dial}, k_{diaN}, k_{diaP}, k_{DiaSi}, k_{flaI}, k_{flaN} and k_{flaP}) are listed in Table 4. Thus, realised diatom growth results from the temperature dependent growth function adjusted by limitations from light and nutrients:

$$g_{dia} = g_{\max} \cdot \lim(I, N, Pho, Sil) \qquad \text{B9.3}$$

N is a weighted sum ($N = Amm + \phi Nit$) of nitrate and ammonium. It is calculated from the variable for nitrogen preference (ϕ, Eq. B1.3.1). Phytoplankton excretion and metabolic losses (*pex*) is assumed to be an exponential function of temperature (see Table 4 for α_{pex} and β_{pex}):

$$pex = \alpha_{pex} \cdot \exp(\beta_{pex} \cdot T) \qquad \text{B9.4}$$

As mentioned above, phytoplankton mortality is simply represented by a parameter (μ). Sinking (*siDia*) is also a source of mortality, and it is represented as a function of diatom and silicate concentrations (see Table 4 for $k_{sidiaMax}$, $k_{sidiaMin}$, k_{sidia} and $k_{silsink}$):

$$sidia = \begin{cases} Dia \cdot k_{sidiaMax} & \text{if } Sil \le k_{silsink} \\ Dia \cdot \left(\dfrac{k_{sidia}}{Sil} + k_{sidiaMin} \right) & \text{if } Sil > k_{silsink} \end{cases} \qquad \text{B9.5}$$

Flagellate biomass (Eq. B10, Table 3) follows similar equations (Eqs B9.1-B9.4), except that they have no silicon requirements and do not sink. Coefficients for growth and affinities (α_{fla}, β_{fla}, α_{fla}, β_{fla}, k_{flaI}, k_{flaN} *and* k_{flaP}, Table 4) also differ from the diatoms.

Grazing on phytoplankton and detritus

The biological model is "closed" at phytoplankton, and phytoplankton mortality from grazing is represented by a constant value (μ). Grazing on phytoplankton and detritus (μ) constitute parts of the respiration by heterotroph organisms. It is assumed that heterotroph growth efficiency *zgreff* depends on temperature:

$$zgreff = \alpha_{zoo} \cdot \exp(-\beta_{zoo} \cdot T) \qquad \text{B10.1}$$

The fraction of grazed phytoplankton and organic material returning directly to the inorganic nutrient pool is:

$$zex = k_{zass} \cdot (1 - zgreff) \qquad \text{B10.2}$$

The rest fraction of grazed material (*1-zex*) enters the detritus pool directly. The return of inorganic ammonium from autotroph and heterotroph excretion:

$$exc(A) = pex \cdot (Dia + Fla) + zex \cdot \mu \cdot (Dia + Fla + DetN) \qquad \text{B10.3}$$

The return of inorganic phosphorous from autotroph and heterotroph excretion:

$$exc(P) = pex \cdot (Dia \cdot r_{diaP} + Fla \cdot r_{flaP}) + zex \cdot \mu \cdot (Dia \cdot r_{diaP} + Fla \cdot r_{flaP} + DetP) \qquad \text{B10.4}$$

The rest of grazed detritus and phytoplankton enters the detritus pool directly. Return to the respective detritus pools (*DetN, DetP and DetS*):

$$grd(N) = (1 - zex) \cdot \mu \cdot (Dia + Fla + DetN) \quad \text{B10.5}$$

$$grd(P) = (1 - zex) \cdot \mu \cdot (Dia \cdot r_{diaP} + Fla \cdot r_{flaP} + DetP) \quad \text{B10.6}$$

$$grd(Si) = \mu \cdot Dia \cdot r_{diaSi} \quad \text{B10.7}$$

Grazed diatoms enter the detritus pool directly, since silicon is not excreted.

Sediment bound processes

Sediment dynamics are represented by three state variables that keeps track of nitrogen (SedN), phosphorous (SedP) and silicate (SedS) concentrations.

Nitrogen in sediments

The nitrogen pool (*SedN*, Eq. B11, Table 3) increases with inputs from diatoms (*sidia*) and detritus (*sidet(N)*) sinking into the sediments. Nitrogen decreases with losses to ammonification (*smir(A)*) and nitrogen (*bur(N)*) being buried in the sediments. Mineralisation of sediment nitrogen (*smir(A)*) is here an exponential function of temperature (*T*) and nitrogen concentration in sediments (*SedN*) (see Table 4 for α_{smir} and β_{smir}):

$$smir(A) = \alpha_{smir} \cdot \exp(\beta_{smir} \cdot T) \cdot \left(\frac{SedN}{Z_b} \right) \quad \text{B11.1}$$

Nutrient concentration in the sediments are given per unit area, and sediment nitrogen (*SedN*) in Eq. B11.1 is divided by the depth interval (Z_b) of the depth cell above in order to get proper units. The fraction of sediment nitrogen buried (*bur(N)*) and permanently lost from the sediment-water system is (see Table 4 for k_{bur}):

$$bur(N) = k_{bur} \cdot SedN \quad \text{B11.2}$$

Ammonium from sediments can enter four different pathways depending on the red-ox state of the sediments (Klump & Martens 1983; Henriksen & Kemp 1988; Koike & Sørensen 1988; Seitzinger 1988; Santschi et al. 1990). At low oxygen concentration a constant fraction (k_{AtoS}, Table 4) will be absorbed into sediment particles and lost from the system (Santschi et al. 1990; Seitzinger et al. 1991). The rest ($1\text{-}k_{AtoS}$) is released as ammonium into water:

$$sedoA = (1 - k_{AtoS}) \cdot q_{SAtoW} \cdot smir(A) \quad \text{B11.3}$$

The variable q_{SAtoW} expresses the influence from sediment red-ox state on the amount of ammonium from sediments (*smir(A)*) being released into the water:

$$q_{SAtoW} = \frac{1}{1 + \left(\frac{Oxy + |Oxy| + 0.1}{|Oxy| + 0.1} \right)^8} \quad \text{B11.3.1}$$

Increasing oxygen concentration stimulates nitrification of sediment ammonium (*smir(A)*), which is released into water as nitrate:

$$sedoN = (1 - q_{SAtoW}) \cdot q_{SNtoW} \cdot smir(A) \qquad \text{B11.4}$$

A fraction of the nitrate ($1\text{-}q_{SNtoW}$) is denitrified and leaves the model system.

$$q_{SNtoW} = \begin{cases} 0 & \text{if } Oxy \le 0 \\ \dfrac{k_{ox}}{1 + \exp(k_{as} - k_{bs} \cdot Oxy)} - k_{cs} & \text{if } Oxy > 0 \end{cases} \qquad \text{B11.4.1}$$

The variable q_{SntoW} expresses the influence from upper sediment red-ox conditions on the amount of nitrate released into water. The coefficients k_{ox}, k_{as}, k_{bs} and k_{cs} are listed in Table 4. The formulations above allow the co-occurrence of nitrification and denitrification (Henriksen & Kemp 1988; Lohse et al. 1993).

Phosphorous in sediments

The phosphorous pool (*SedP*, Eq. B12, Table 3) increases as diatoms (*sidia*) and detritus (*sidet(P)*) sink into the sediments. The pool decreases with losses to mineralisation (*smir(P)*) and burial (*bur(P)*) phosphorous compounds. Some of the mineralised phosphorous is absorbed (*seqP*) by sediment particles. Phosphorous mineralisation follows the same equation as nitrogen (s*mir(A)*, Eq. B11.1. The fate of mineralised phosphorous (*smir(P)*) depend on the red-ox state of the sediment (Caraco et al. 1989; 1990; Santschi et al. 1990; Sundby et al. 1992). At aerobic conditions a fraction (q_{PtoS}) of the mineralized phosphorous is adsorbed into solid sediment particles:

$$seqP = q_{PtoS} \cdot smir(P) \qquad \text{B12.1}$$

The rest fraction ($1\text{-}q_{PtoS}$) of is released into water:

$$sedoP = (1 - q_{PtoS}) \cdot smir(P) \qquad \text{B12.2}$$

The fraction of phosphorous sequestered and released from the sediment depends on oxygen conditions in the sediment:

$$q_{PtoS} = \frac{k_{aer} \cdot Oxy}{k_{ana} + Oxy} \qquad \text{B12.3}$$

Silicate in sediments

The silicon pool (*SedSi*, Eq. B13, Table 3) increases as diatoms (*sidia*) and detritus (*sidet(Si)*) sink into the sediments. The pool decreases with losses to mineralisation (*smir(Si)*). Mineralisation of sediment silicon (*smir(Si)*) is expressed by similar equations to nitrogen (Eq. B11.1), only substituting nitrogen with silicon.

Oxygen

Oxygen is consumed in the process of aerobic decomposition (mineralisation) of organic matter and in the nitrification of ammonium:

$$sedres = k_{detO} \cdot smir(A) + k_{nitrO} \cdot sedoN \qquad \text{B14}$$

Implementation of the model

Golfo Dulce and the adjacent coast are divided into a 66 by 48 horizontal grid net with a 2 by 2 km^2 grid resolution (Figure 4). The model map is rotated in order to get the landside of the coastline running parallel to the x-axis of the model. This means that the onshore/offshore direction runs parallel to the y-axis of the model (Figure 4). Some of the variables of the model (wind, currents) are directional and defined by vectors in the x, y, z ordinate system of the model. The reader should notice that all references of directions in the following refers to the model map directions (x,y,z). The directional values (+/-) of the x- and y-vectors are shown in Figure 4. The z-vector is positive in the upward direction (towards surface). The vertical dimension is divided into 24 sigma layers, ranging from 0 to 1, where 0 and 1 represent surface and bottom, respectively. The ocean boundaries interact with the model through a *Flow Relaxation Scheme*, FRS (Martinsen & Engedahl 1987), in the outer 10 grid cells. The FRS zone dampens feedback effects and drags the modelled variables towards the ocean boundary values.

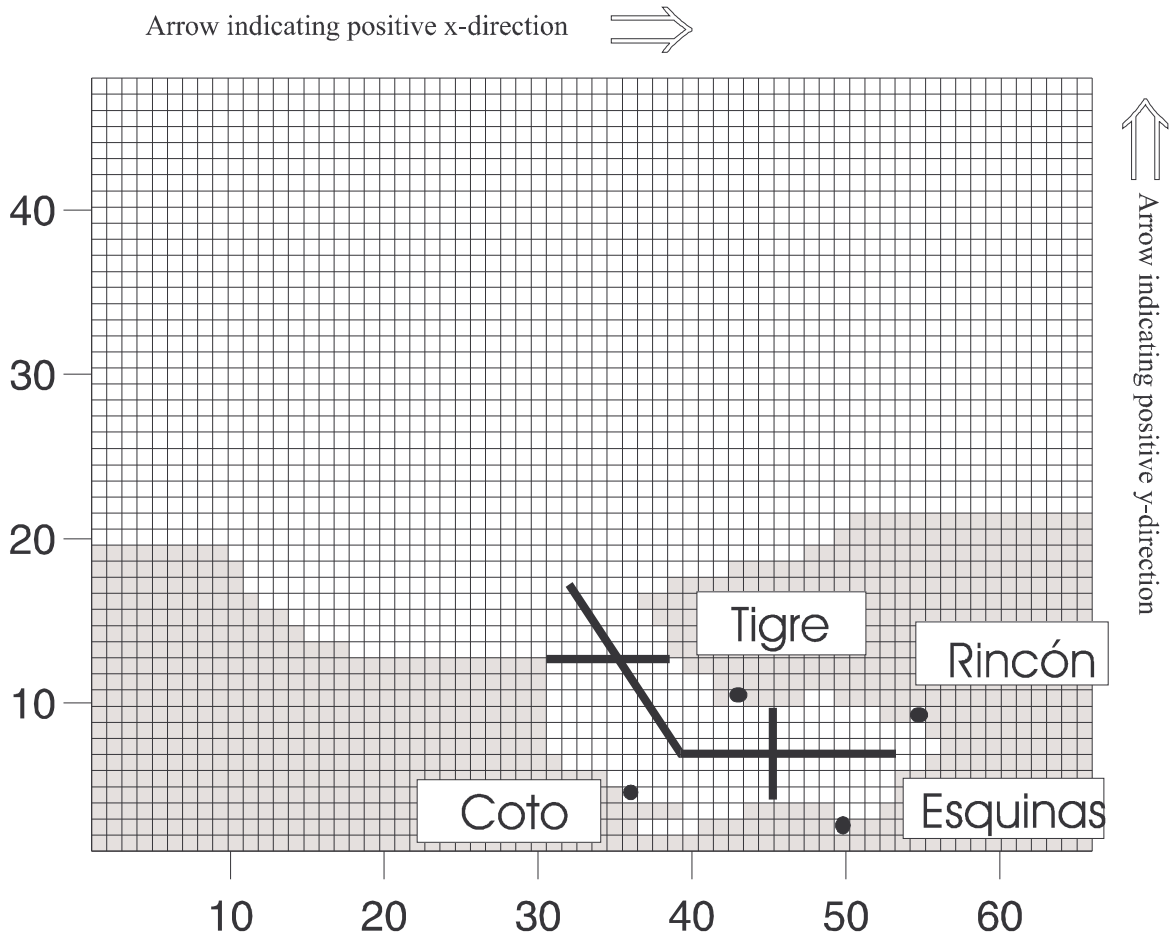

FIGURE 4. The rotated map as implemented in the model, with the horizontal grid cells and land contours. The circles on the map mark the position of the four main rivers entering the gulf. The lines mark the location of the vertical sections of the figures presented in the results

External forcing

The external forcing functions are represented by surface wind, air-sea heat flux, freshwater and ocean boundaries as illustrated in Figure 2.

Bottom topography

Bottom topography (Figure 5a, b) influences the bottom currents through frictional forces. The original bottom matrix is smoothed in order to avoid too steep depth gradients between adjacent grid cells.

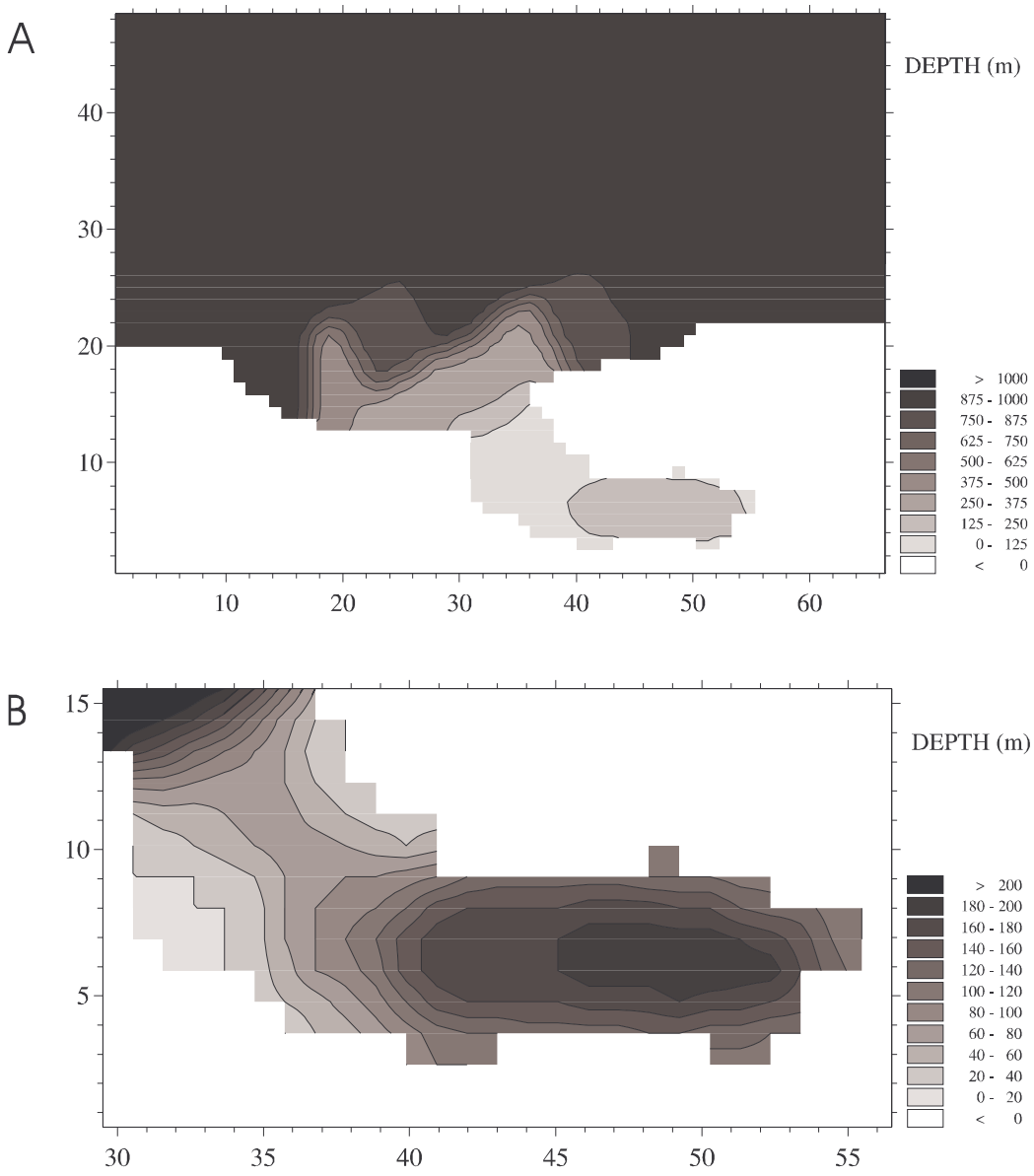

FIGURE 5 A: The bottom topography of the total model area **B:** The bottom topography of Golfo Dulce. The scales to the right show the depths corresponding to each contour

Surface wind

Surface wind (Figure 6) is based on wind fields from the Equatorial Pacific (Oort 1983). These wind data represent monthly averages of a meridional and zonal wind components. Wind is implemented on surface grid cells as two horizontal speed components, x- and y-components (Figure 4). Wind is not spatially resolved, i. e. all surface grid cells are forced by the same wind field at the same time.

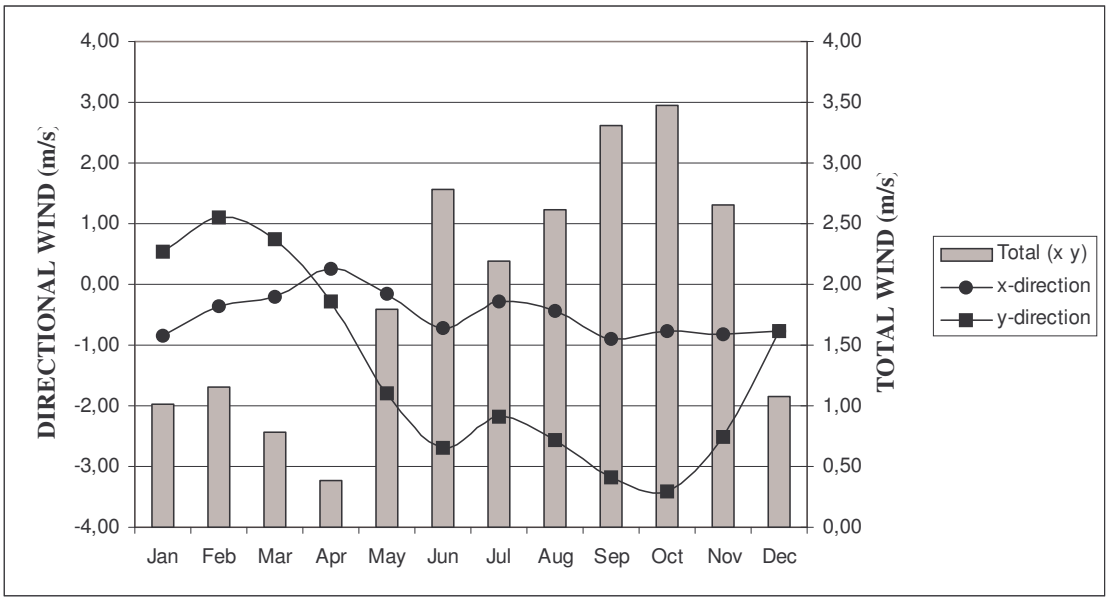

FIGURE 6. Monthly wind fields used to force the model. The lines show the x, y-vector components (m/s) of wind. Bars present total surface wind (m/s) calculated as the vector product of the x and y wind components

Air-sea heat flux

Air-sea heat fluxes are approximated by a calibration of sea temperatures in the surface grid cells. The calibration procedure drags modelled surface temperature towards observed (Levitus and Boyer 1994b) surface temperature:

$$\Delta T = k_T \cdot \left(T_{obs} - T_{mod}\right) \qquad \text{(a)}$$

$$T = T_{\mathrm{mod}} + t_s \cdot \Delta T \cdot \left(D_{x,y} \cdot \partial z_1\right)^{-1} \qquad \text{(b)}$$

Here ΔT (°C m/s) is the difference between observed (T_{obs}, °C) and calculated (T_{mod}, °C) surface temperatures, k_T (m/s) is the calibration constant with the value $1.736 \cdot 10^{-5}$, T (°C) is the calibrated surface temperature, t_s (s) is the time step of the model, $D_{x,y}$ (m) is the dynamic bottom depth at x,y and ∂z_1 (dimension less) is the thickness of the surface sigma layer.

A

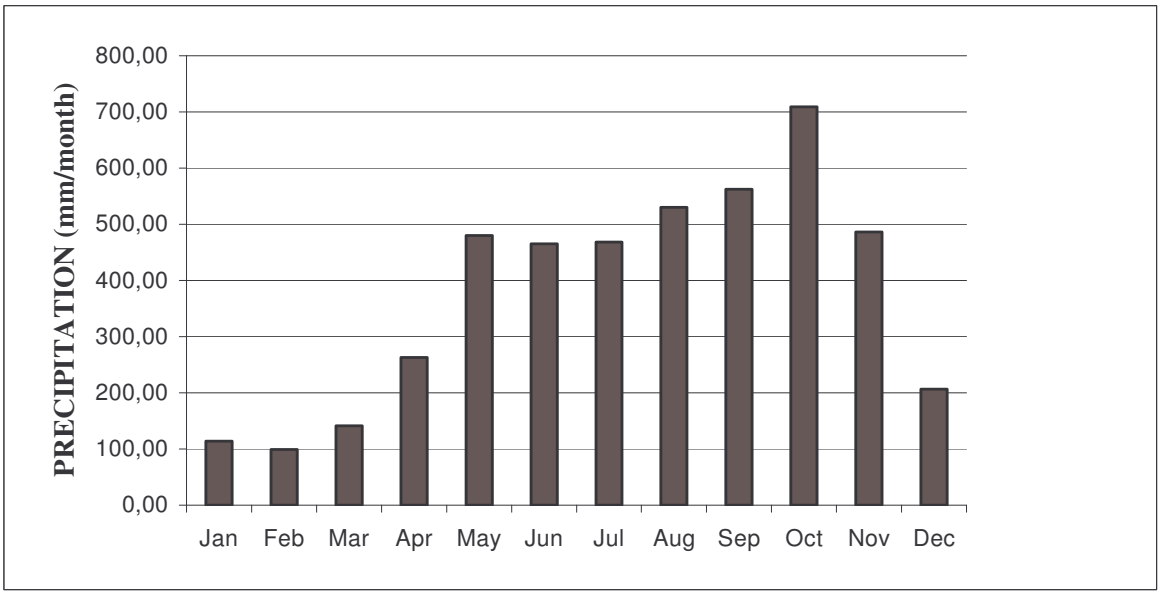

B

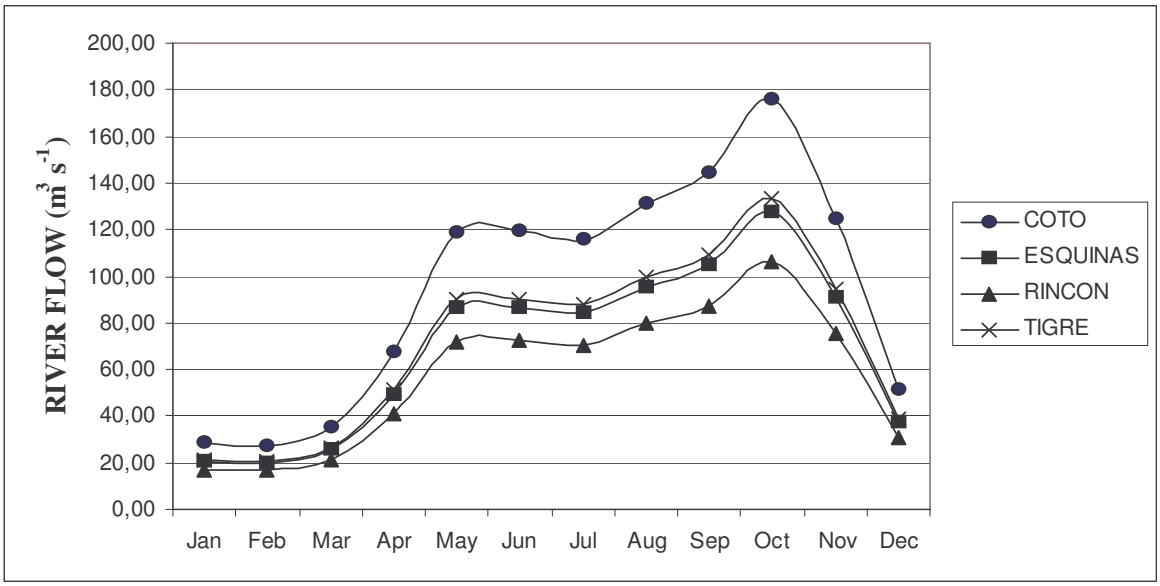

FIGURE 7. A: Monthly precipitation (mm/month) in the catchement basin of Golfo Dulce **B:** Estimated monthly freshwater transport in the four main rivers, Coto, Tigre, Esquinas, Rincón, entering Golfo Dulce

Freshwater runoff

Freshwater entering the gulf is calculated from monthly precipitation (Figure 7) in the catchement basin of Golfo Dulce (Herrera 1985). Freshwater flow is channelled into four main rivers, and monthly precipitation is transformed to flow per unit time (m^3/s). Total freshwater inflow to the catchment basin is distributed in the four main rivers (Coto, Tigre, Esquinas and Rincón) by a formula obtained by dividing the coastlines on each side of the river mouths by the total coastline inside Golfo Dulce. The argument for this was that coastline may serve as a measure of the land areas catching up the precipitation that finally ends up in the rivers. This procedure yields a flow relationship of 32:24:23:21 between Coto, Tigre, Esquinas and Rincón, respectively. Each of the rivers are implemented as one horizontal grid cell (Figure 4), and the flow is given as volume per second in a given direction along the *x* or *y* axis of the model. Temperatures and chemical variables of the river water is based on data from the Coto river system (Michels unpubl. data), and include estimates of nitrate, phosphorous and silicon.

Tides

Tidal energy acts on the ocean boundaries and is represented by surface elevation (m) and tidal currents (m/s). Tidal currents run along the x-axis (Figure 4). Tidal amplitudes are based on 1980 data from the station Quepos on the Pacific coast of Costa Rica (Gutierrez unpubl. data). Due to bottom effects near the shore these data are probably not representative for the tidal amplitudes at the model boundaries off the coast. The observed tidal amplitudes were, therefore, scaled down to get more realistic amplitudes off the coast. The scaling factor was adjusted to get the average tidal amplitudes (mean of observed values) off the coast about 0.7 m. Tidal currents are calculated from surface elevation, assuming a depth about 1000 meters in the boundary zone.

Ocean boundaries

Salinity and temperature at the ocean boundaries are based on monthly data from the Equatorial Pacific (Levitus and Boyer 1994b). The temperature data provided values above 50 meters only. Temperature was, therefore, extrapolated towards 10°C at 1000 m. Continuos salinity and temperature data at the ocean boundaries are obtained by linear interpolation of the monthly data.

There are no data on coastal currents along the coast of Costa Rica, and the tidal currents are the only currents represented at the ocean boundary.

Chemical and biological variables at the ocean boundary are represented by annual values of nitrate, phosphorous, silicate (Conkright et al. 1994, Levitus et al. 1994) and oxygen (Levitus and Boyer 1994a). The oceanic concentrations of ammonium and detritus are set to zero, while phytoplankton are given the value 1mgN m^{-3} for depths above 50 meters, and zero for depths below 50 meters.

Initialisation

The model is initialised with conditions corresponding to the vertical structure at the oceanic boundaries (Levitus and Boyer 1994a, b; Levitus et al. 1994). The sediments are initiated with concentration of nitrogen, phosphorous and silicon listed in Savchuk and Wulff (1996).

Simulations

The model was tested in four annual scenarios with different external forcing. In the basic run all the natural forcing functions are active. In order to study the influence from the different forcing functions (wind, freshwater and tide), each of these was left out in separate simulations. The basic run is used as standard for comparisons of the other three simulations. The basic run also represents the standard for real world comparisons. Since forcing data are based on monthly averages, the model output is presented as monthly averages. The annual simulations are all initiated on January the 2nd.

Three other simulations with a monthly horizon demonstrate the effects from inorganic substances and river nutrient on primary production.

Results

Some of the figures presented below refer to vertical sections from Golfo Dulce. These sections are shown in Figure 4 for reference.

Circulation

The basic run predicts an estuarine circulation pattern, with outflowing brackish water near the surface, and inflowing oceanic water between 5 to 30 meters in the sill area (Figures 8-10). The vertical location and extension of in- and outflowing water, changes with season (Figures 9-10). Relatively strong currents in the sill area and weaker currents towards the inner and deeper gulf seem to be the general pattern for all seasons (Figures 8-9). Vertical cross sections in the central gulf (Figure 11) show a clockwise circulation pattern inside the gulf (the horizontal plane). Inflowing currents dominate most of the northern (referring to model north in Figure 4) gulf, the deeper and central basin during the wet season (Figure 11). The in- and outflowing currents have more clear-cut vertical boundaries in the central gulf during the dry months in early spring (Figure 11). Barotropic effects from inflowing freshwater in combination with bottom topography may explain the predicted clockwise circulation pattern in Golfo Dulce.

Freshwater inflow is most dominant during the rainy season from May to November (Figure 7), and is evident as a thicker outflowing brackish surface layer during these months (Figure 9 and 12). Inflowing freshwater reduces surface salinity and creates a distinct halocline from June to October (Figure 12).

Surface winds (Figure 6) blow onshore during most of the rainy season, and seems to partly counter the freshwater driven outflow near the surface in this period (Figure 8). The winds blow offshore during the dry season, and combined with freshwater, creates a relatively strong outflowing surface current in February. The outflowing surface layer is thinner in February (Figure 9) compared to the wet months. Wind forcing is most powerful during the rainy season, with a maximum peak around October (Figure 6). The wind effect on surface currents is most evident in the ocean area during these months (Figure 8). Surface currents in the areas outside the gulf seem more evenly influenced by wind and freshwater outflow from the gulf (Figure 8). The direction of surface currents is less clear in this area. The opposite situation occurs in February, where both wind and freshwater flow tend to flush gulf water offshore (Figure 8).

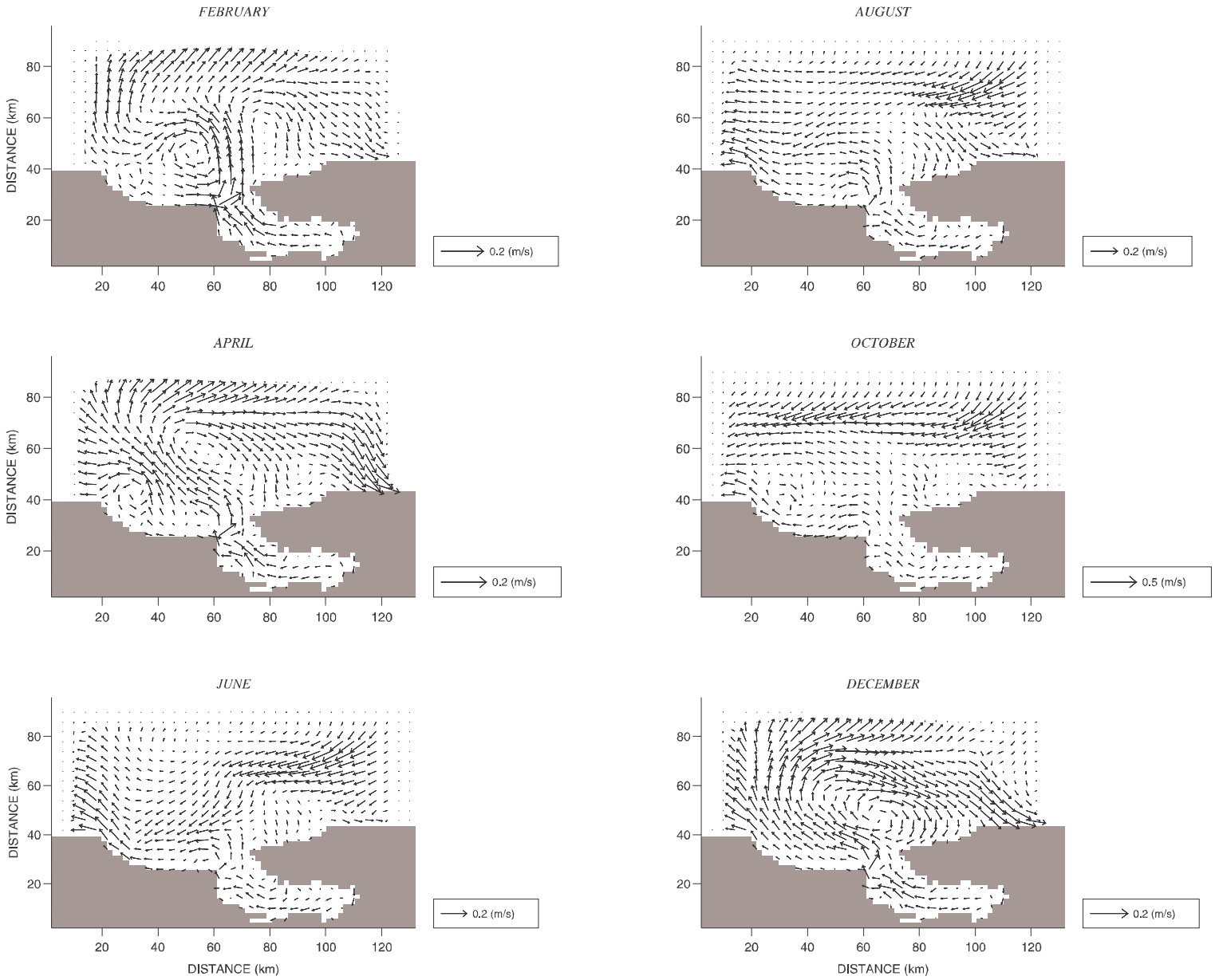

FIGURE 8. Predicted average monthly horizontal surface currents (m/s) in the basic run. The legends to the right show the value corresponding to the length of the vectors

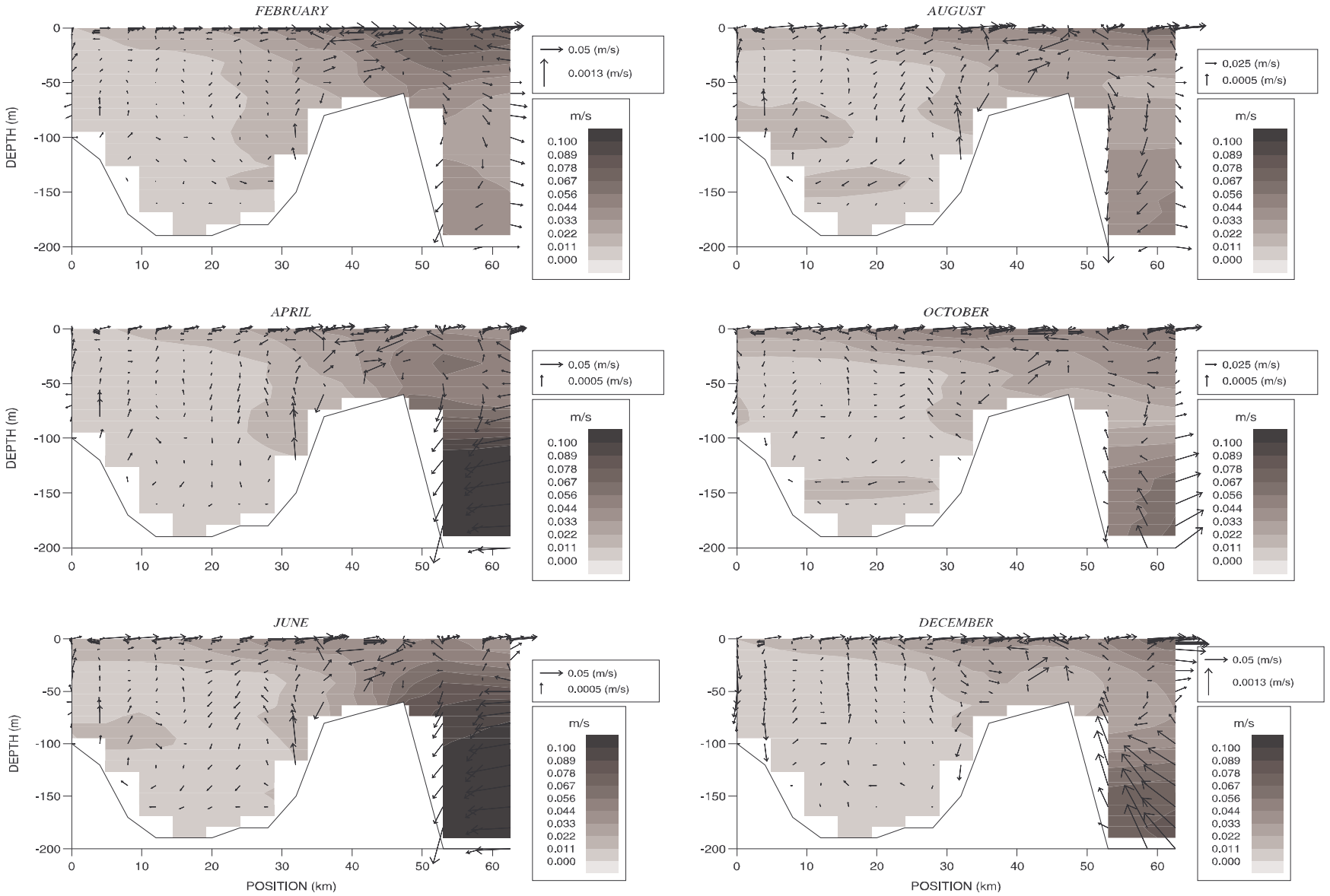

FIGURE 9. Predicted average monthly currents in the basic run. The figures show a vertical section (see Fig. 4) in the length direction along the central Golfo Dulce. The vectors show the direction of current components (m/s) in the plane of the section. The contour plots show the product of all vector components (x, y, z). Because of the large difference between horizontal and vertical currents, the vectors represent different values (as indicated by the vector legends). The scales to the right show the values corresponding to each contour

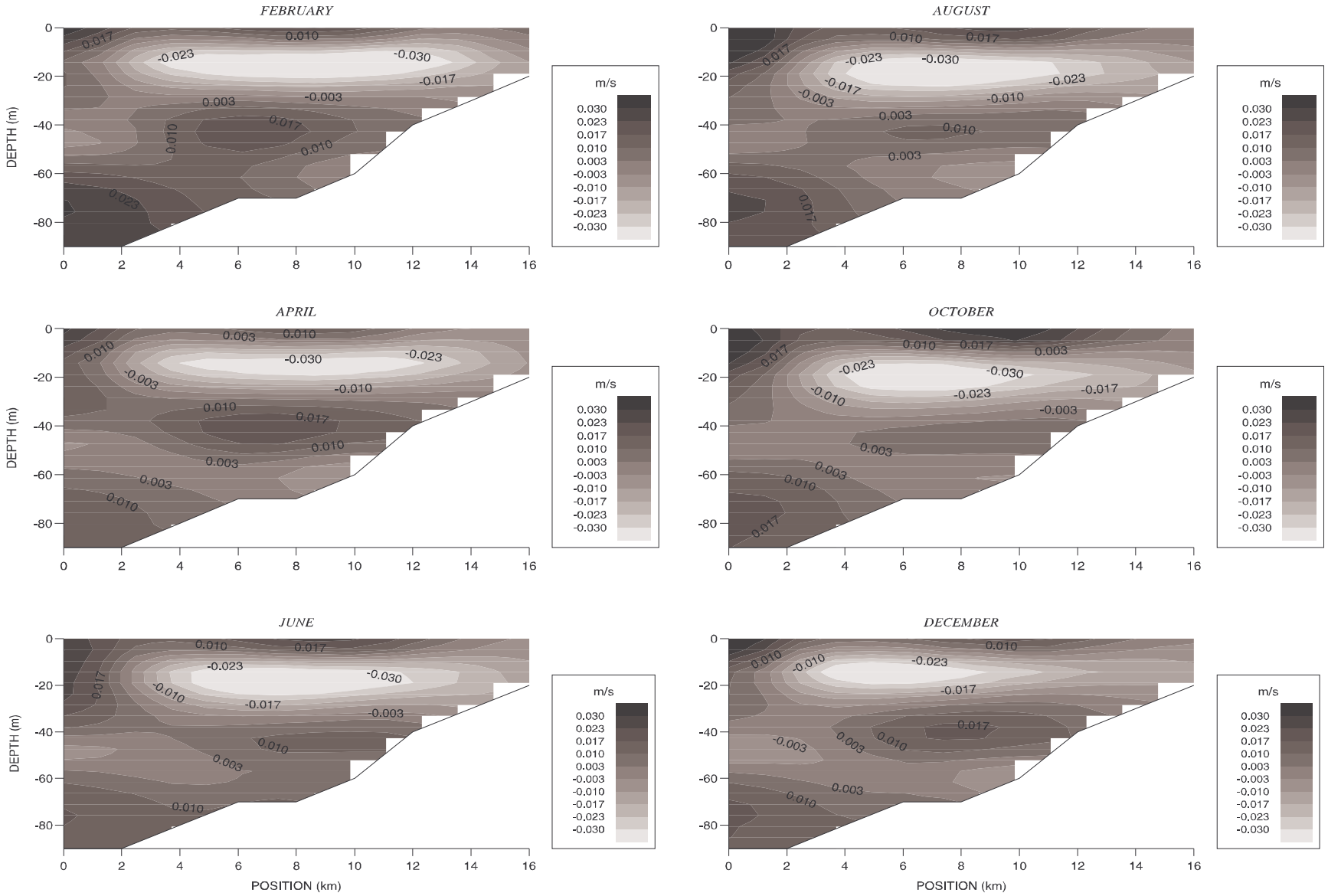

FIGURE 10. Predicted average monthly currents in the basic run. The figures show a vertical section across the sill (see Fig. 4), looking out of the gulf. Contours show the value of the vector component perpendicular to the plane of the section. Negative and positive values indicate in- and outflowing currents, respectively. The scales to the right show the value of contours (m/s)

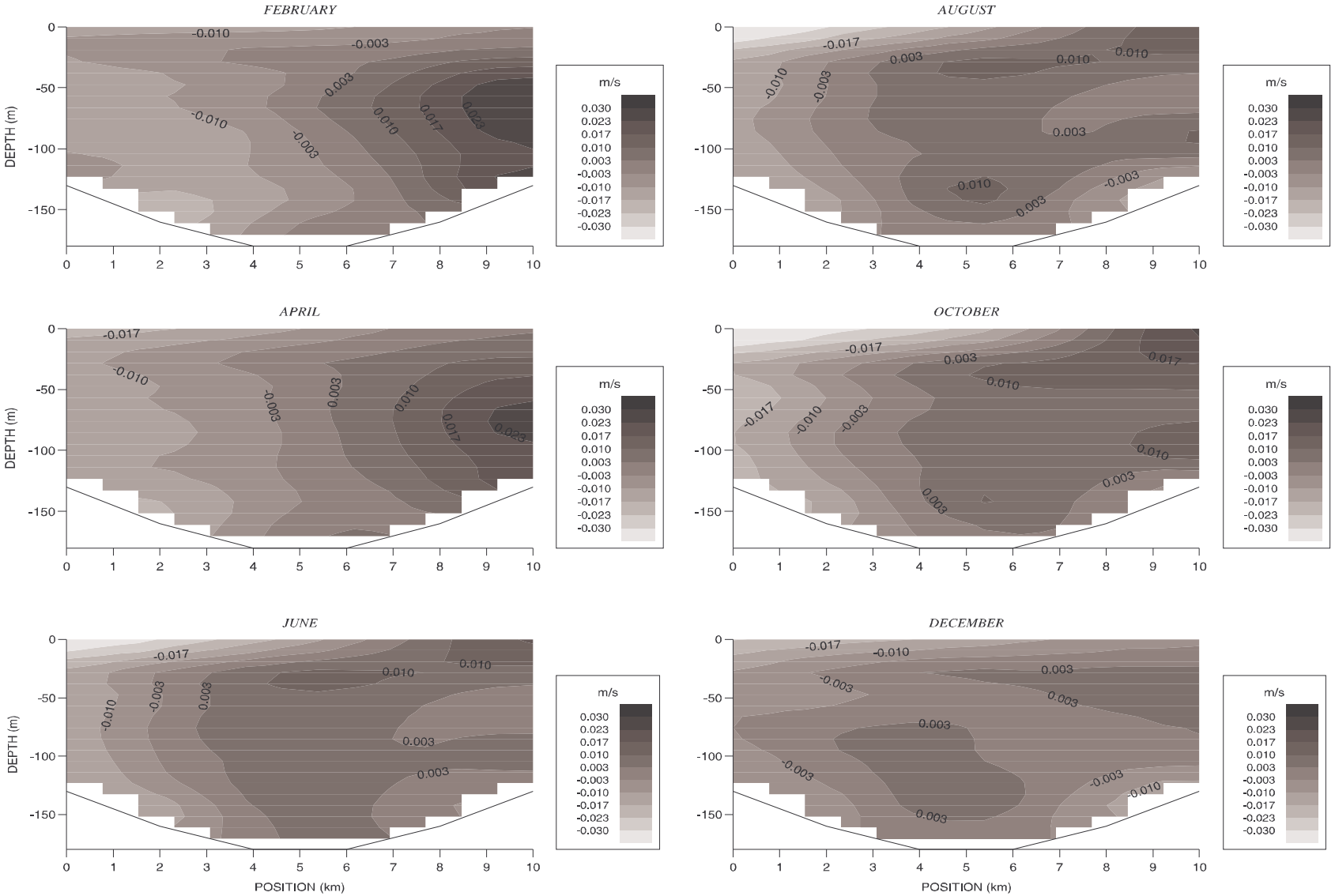

FIGURE 11. Predicted average monthly currents in the basic run. The figures show a vertical cross section (see Fig. 4) near the center of the gulf, looking towards the gulf entrance. Contours show the value of the vector component perpendicular to the plane of the section. Positive and negative values indicate in- and outflowing currents, respectively. The scales to the right show the value of contours (m/s)

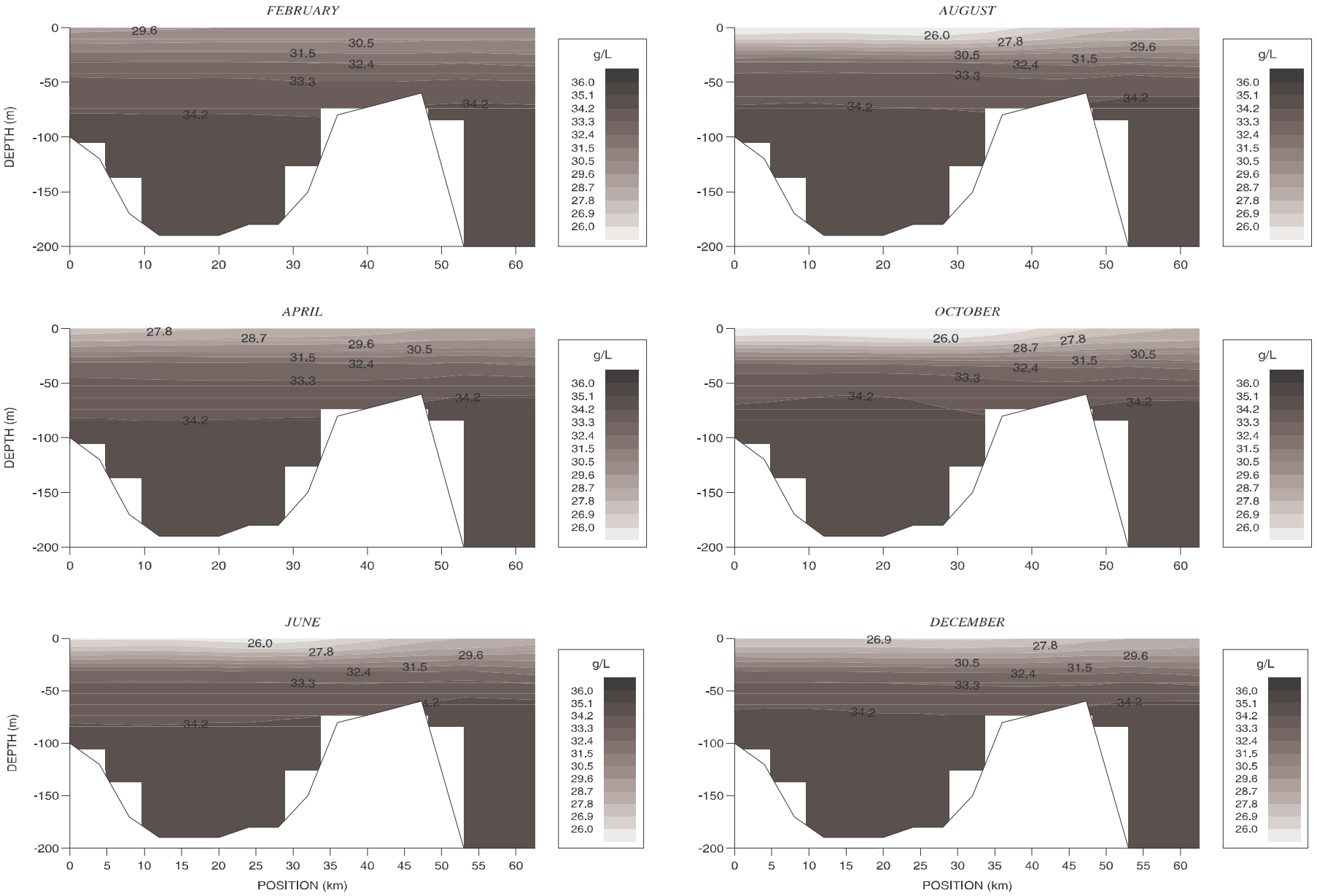

FIGURE 12. Predicted average monthly salinity in the basic run. The figures show a vertical section (see Fig. 4) in the length direction along the central Golfo Dulce. The scales to the right show the values corresponding to each contour (‰)

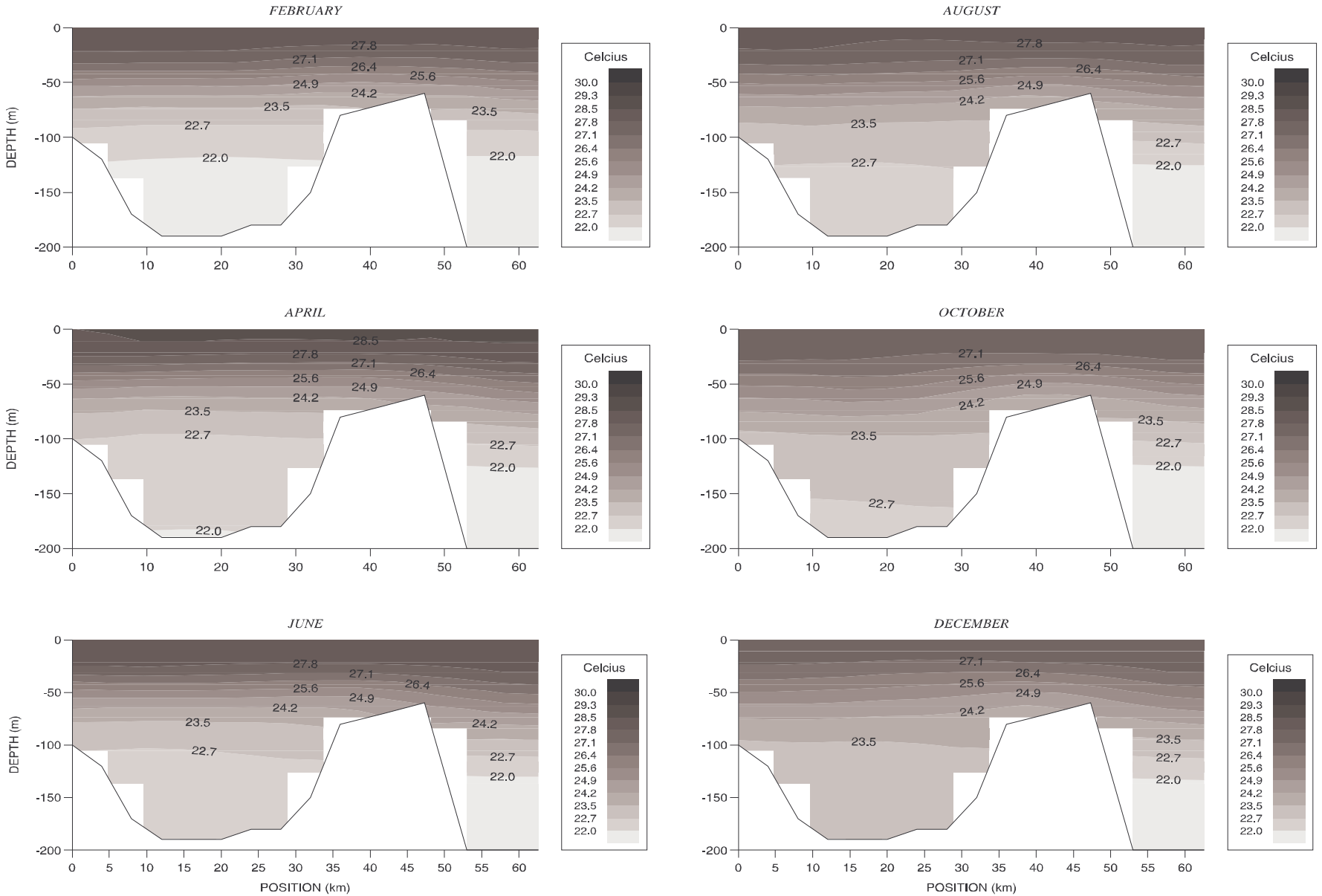

FIGURE 13. Predicted average monthly temperatures in the basic run. The figures show a vertical section (see Fig. 4) in the length direction along the central Golfo Dulce. The scales to the right show the values corresponding to each contour (°C)

Hydrography

The vertical salinity profiles (Figure 12) seems to be relatively stable below 30 meters in all seasons. Above 30 meters, however, salinity changes according to seasonal variation in freshwater. During the rainy season, surface salinity is low with a strong surface salinity gradient (Figure 12). The surface layer is well mixed with smother surface salinity gradients, during the dry season (Figure 12).

During the rainy season, surface temperature (Figure 13) is cooled slightly by river water. Temperature evolution in the deeper inner gulf indicates that there occurs a vertical mixing between shallow and deep water. This creates warmer deep-water in the inner gulf towards the end of the annual simulation (Figure 13) compared with the initial conditions. Vertical currents (Figure 9) also indicate a vertical mixing of water below the sill depth, which is probably influenced by the estuarine circulation above sill depth.

Inorganic nutrients

The vertical profiles of nitrate, phosphorous, silicon, ammonium, oxygen and detritus change relatively little across the seasons. The October situation (Figure 14) is used to illustrate the distribution of the variables. Except for ammonium, the vertical profiles of inorganic nutrients are in general characterised by low concentrations in the euphotic zone, and increasing concentrations with depth (Figure 14). The distribution of ammonium, which represents regenerated nitrogen nutrients, is similar to that of diatoms (Figure 14). Thus, predictions indicate that metabolic "leakage's" from phytoplankton cells are the main source of ammonium. Ammonium concentrations are, however, very low compared to nitrate.

The biological model has to go through an initial stabilisation phase, where the level of inorganic nutrients and phytoplankton adjusts. A strong initial phytoplankton growth combined with a drop in nutrient concentrations near the surface is evident in Figure 15. It is also evident (Figure 15) that nutrient concentration in the deeper water increase during the simulation. This is partly a result of mineralisation of detritus particles that have sunk out from the euphotic zone (Figure 14), and partly a result of oceanic "pumping" of nutrients into the gulf via the estuarine circulation (Figure 9). Nutrient concentrations near the surface are more fluctuating (Figure 15), and seem to depend more upon nutrient consumption by phytoplankton. Peaks in the coastal water currents outside the gulf seem to cause the strong peaks in nutrients concentrations near the end of the simulation (Figure 15). The currents generate an inflow of nutrient rich water to the gulf (Figure 9).

Phytoplankton

The spatial distributions of diatoms and flagellates in the gulf are different. Diatoms are in general located deeper, and with the highest densities in the sill area (Figure 16). Flagellates are more surface oriented (Figure 17), and seem to have a more even horizontal distribution. The differences in distribution may be explained by the higher diatom affinity for light and nutrients, and a higher growth potential compared to the flagellates. This enables diatoms to outgrow flagellates under all conditions except under silicate limitation. The low silicate concentrations near surface restrict diatom growth inside the gulf, and enables a flagellate dominated phytoplankton community near the surface. However, silicate concentration increases with depth to satisfactory conditions for diatom growth.

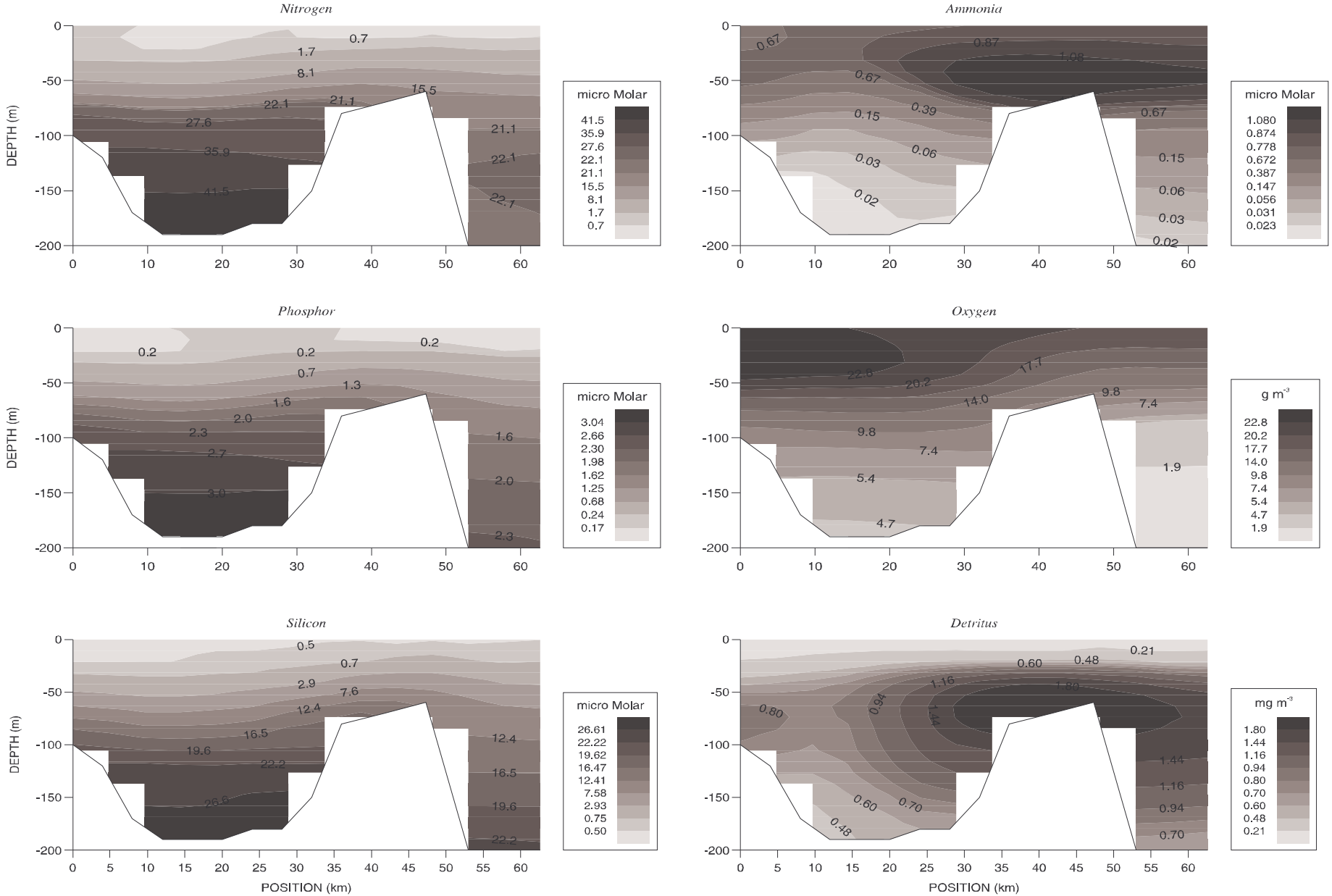

FIGURE 14. Predicted average monthly concentrations of inorganic nutrients (nitrogen, phosphor, silicon, ammonia), oxygen and detritus in October. The figures show a vertical section (see Fig. 4) in the length direction along the central Golfo Dulce. The scales to the right show the values corresponding to each contour

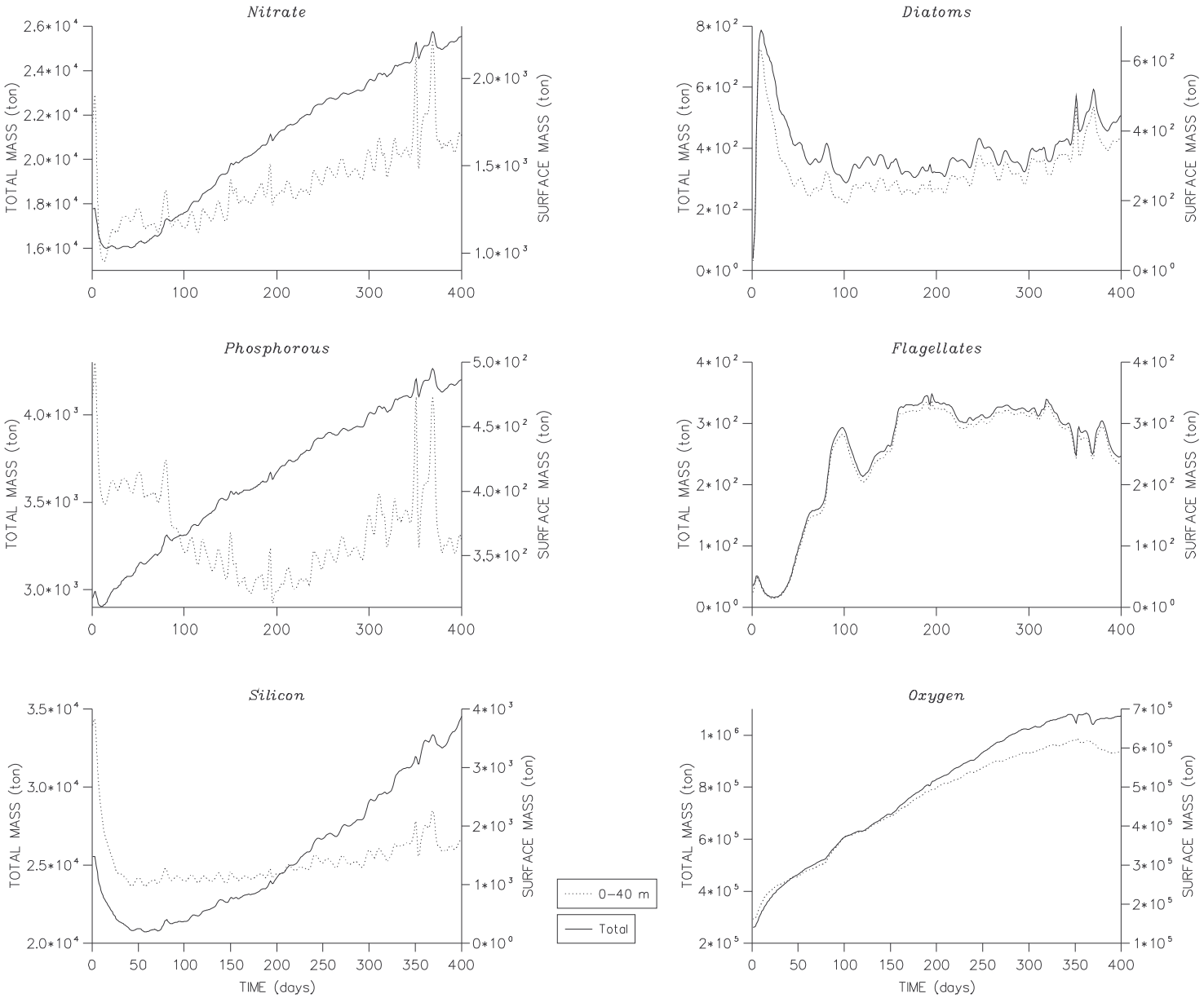

FIGURE 15. Predicted average daily (24 hrs) amounts (tons) of nitrogen, phosphor, silicon, diatoms (in nitrogen equivalents), flagellates (in nitrogen equivalents) and oxygen in Golfo Dulce. The two lines represent surface (upper 40 meters) and total mass (surface to bottom) of the different elements

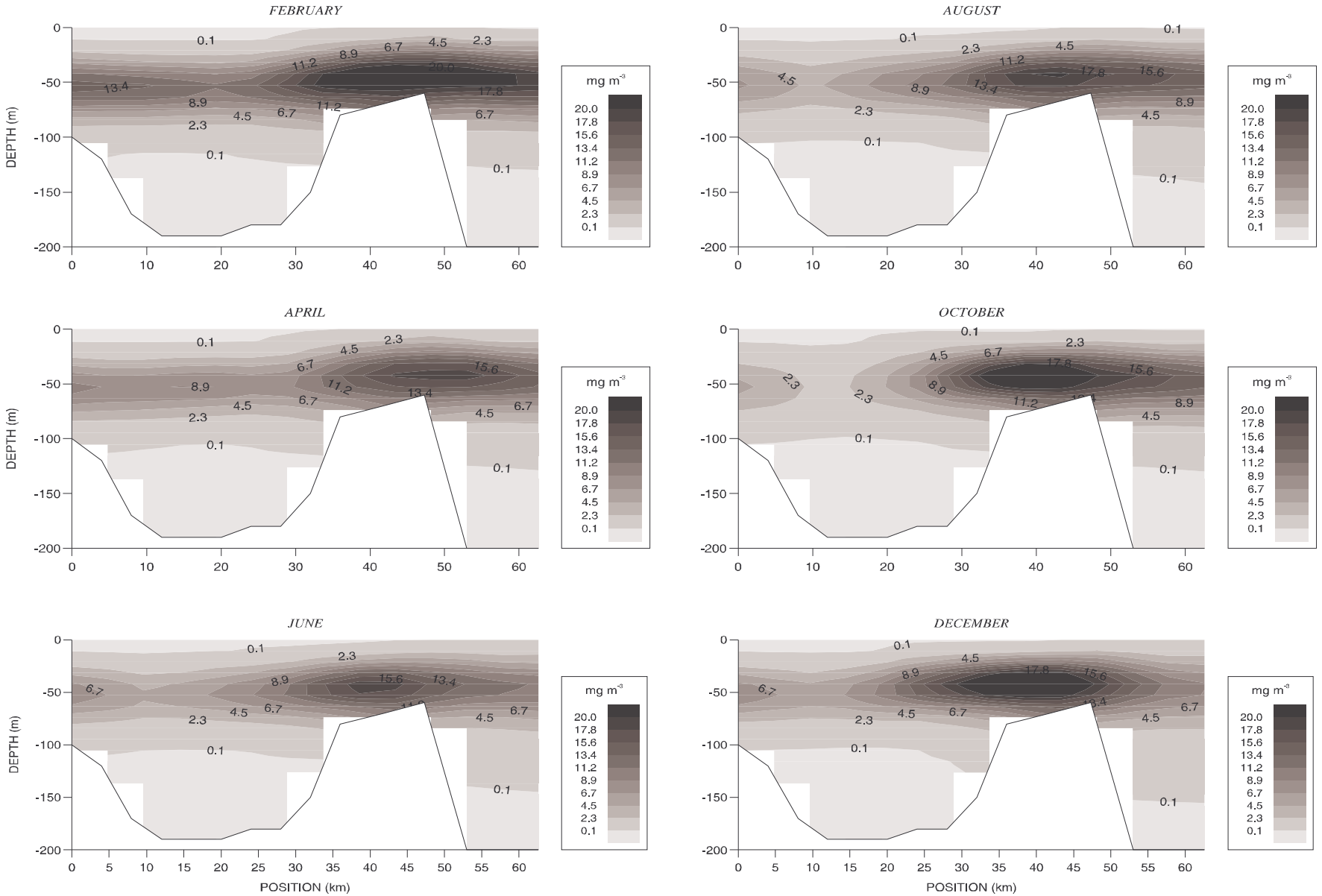

FIGURE 16. Predicted average monthly concentrations (in nitrogen equivalents) of diatom phytoplankton. The figures show a vertical section (see Fig. 4) in the length direction along the central Golfo Dulce. The scales to the right show the values corresponding to each contour

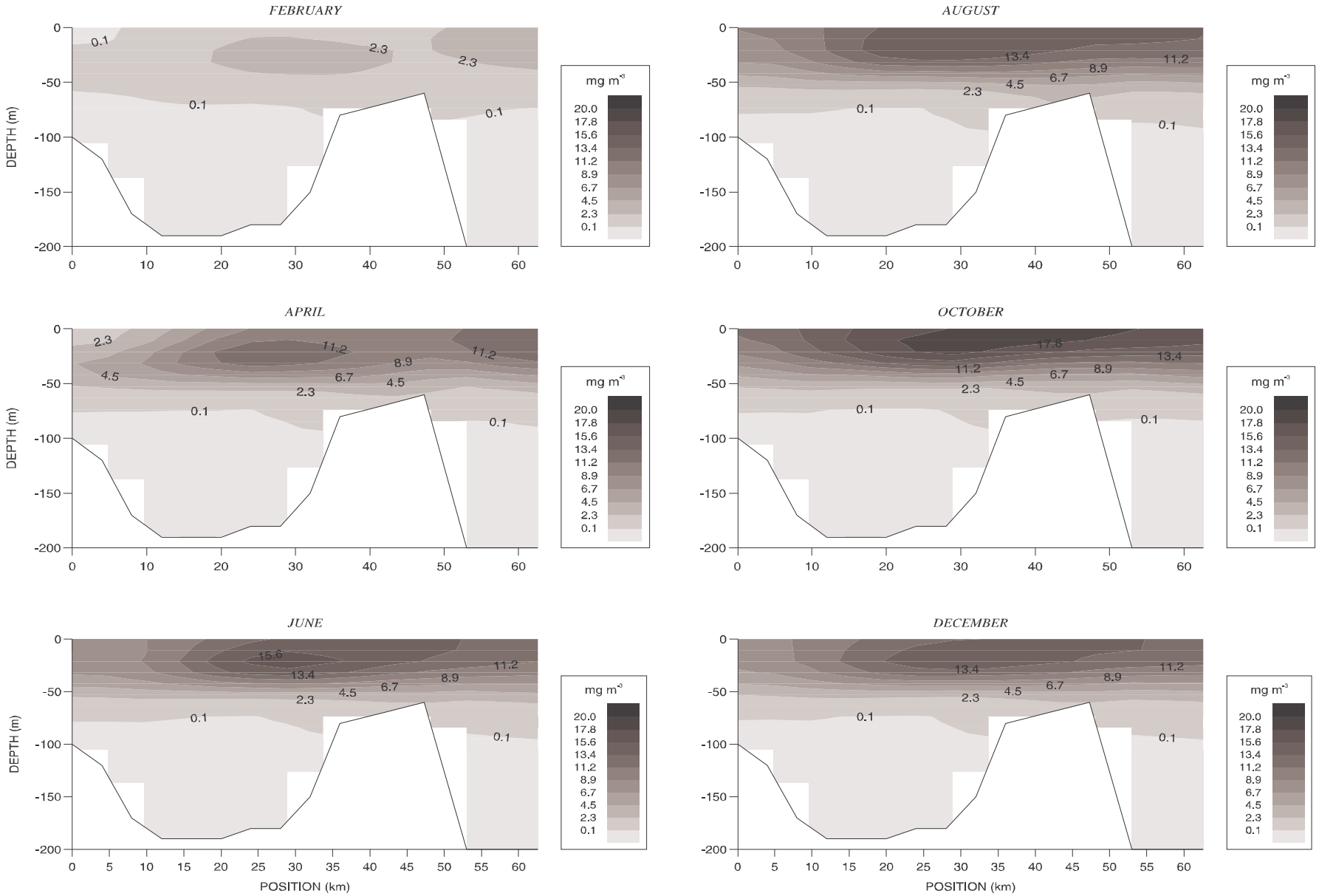

FIGURE 17. Predicted average monthly concentrations (in nitrogen equivalents) of flagellate phytoplankton. The figures show a vertical section (see Fig. 4) in the length direction along the central Golfo Dulce. The scales to the right show the values corresponding to each contour

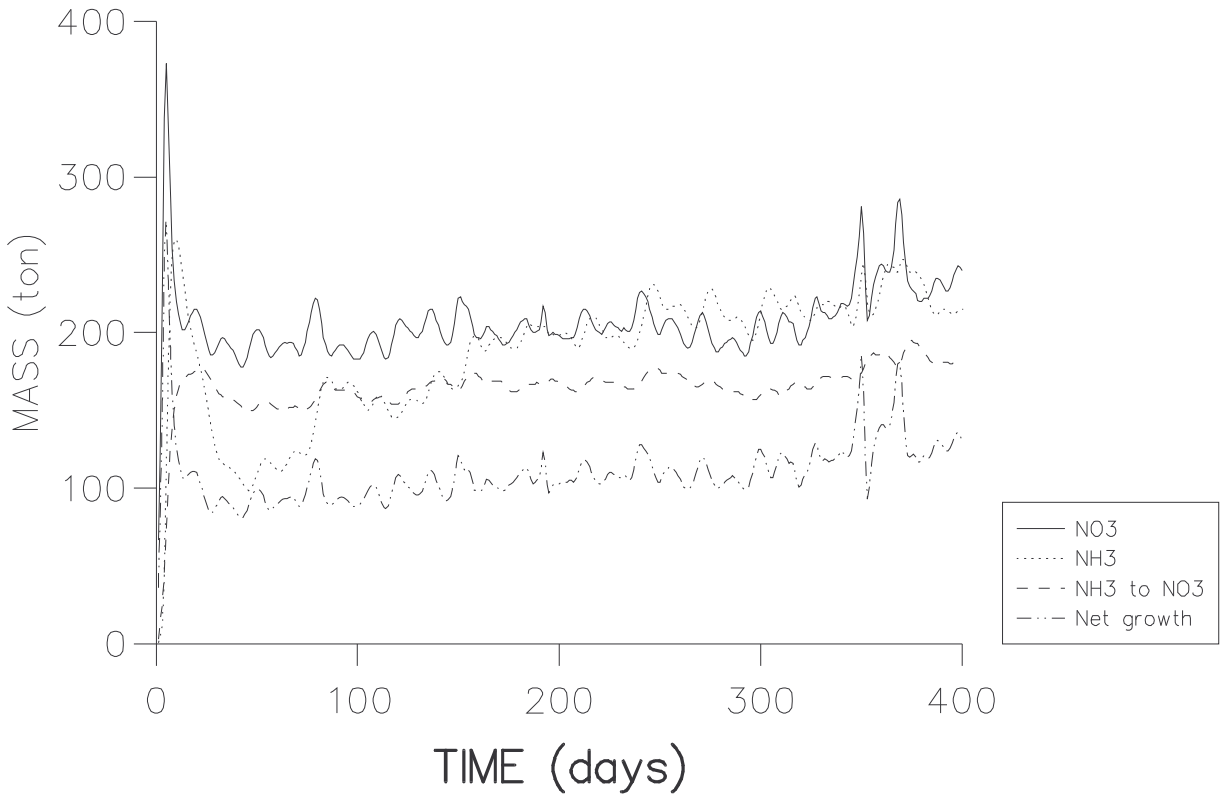

FIGURE 18. Predicted daily (24 hrs) phytoplankton uptake of different nitrogen sources (nitrate or ammonia), nitrification of ammonia (tons) and net growth of phytoplankton in Golfo Dulce

The best growth conditions, which is a balance between nutrients (increasing with depth) and light (decreasing with depth), seems to be around 50 meters in the inner gulf (Figure 16). The higher diatom concentration near surface in the sill area is probably connected to the turbulent mixing in this area (Figure 9). Turbulent mixing brings nutrient rich water to the surface, and combined with better light conditions, this provides better growth conditions for diatoms compared to the inner gulf (Figure 16).

Nutrient peaks near the end of the simulation also affect phytoplankton biomass (Figure 15). Diatom biomass has peaks corresponding to peaks in nutrients, while peaks in flagellate biomass are negatively correlated with the nutrient peaks (Figure 15). Due to their surface near location, flagellates are transported out of the gulf as a consequence of the estuarine circulation. The deeper located diatoms, on the other hand, are transported into the gulf.

Ignoring initial noise, the net phytoplankton production (Figure 18) stays at fairly constant levels during the simulation (about 100 ton nitrogen each day inside Golfo Dulce).

Oxygen

Oxygen concentrations increase during the simulation (Figure 15). The rate of increase, however, decreases towards the end of the run. This indicates that production and consumption are approaching each other through out the run. Highest concentrations occur in the surface areas in the inner gulf (Figure 14). This is probably the result of a transport of oxygen along the incoming estuarine counter current (Figure 9). Anoxia occurs initially in some of the bottom cells (not evident from any of the present figures). However, oxygen from photosynthetic production near the surface is mixed downwards at rates exceeding the oxygen consumption in the deep waters.

Detritus

Detritus seems to follow a similar vertical distribution pattern as the diatoms, although the maximum concentration of detritus is located deeper (Figure 15). Detritus does not accumulate in depth because the mineralisation rates exceed the sinking rates (Figure 14).

New and regenerated production

Nitrate seems to be the dominating nitrogen source during the first third of the simulation (Figure 18). Thereafter nitrate and ammonium contributes almost equal amounts to phytoplankton production. Ammonium nitrified to nitrate contributes about 80 percent of the nitrate consumed by phytoplankton (Figure 18). This indicates that most of the production is regenerated. The model is, however, unable to trace the origin of nitrate, i. e. whether it is regenerated in the gulf or originates from coastal or river water. The accumulation of nutrients in depth combined with decreasing detritus concentrations in depth indicate that most of the nitrified ammonium ends up as nitrogen in the deeper gulf water. Therefore, most of the nitrogen consumed by phytoplankton is probably of coastal and river origin, and as such, represents new production. Peaks in nitrate uptake (Figure 18) near the end of the simulation support the idea that local upwelling of nutrient rich water at the sill creates the unexpected peak in diatom biomass (Figure 15) discussed above.

Sediment nutrients

Sediment nutrient concentrations (Figure 19) increase steadily along the run, meaning that inputs to sediments (sinking) are higher than the outputs (mineralisation processes).

Sensitivity to natural forcing functions

The relative importance of the main natural forcing, freshwater runoff, wind and tides, was evaluated by comparing the differences (Figures 20a, b) between selected variables in the basic run, and the runs where these forcing functions were left out. The deviation ($d_{c,v}$) from basic run, induced by changes in the forcing function c, is calculated as the sum of deviations (v_c) in variables from all position ($n = 1, N$) at different time periods ($m = 1, M$):

$$d_{c,v} = \sum_{n=1}^{N} \sum_{m=1}^{M} \left| v_c(n,m) \right|$$

The relative influence (D_y) from different forcing functions (c) on the variable v_c are calculated as:

$$D_v = d_{c,v} \cdot \left(\sum_{c=1}^{C} d_{c,v} \right)^{-1}$$

The comparisons are grouped between variables above 10 meters (Figure 20a), where wind and river flow are expected to be most influential, and variables below 10 meters (Figure 20b) where wind and rivers are probably less influential on circulation.

Wind seems to have the less influence on variables inside Golfo Dulce, contributing only about 20% of the total variation (Figures 20a, b).

Freshwater seems to have more influence, contributing roughly between 20-70% of total variation (Figures 20a, b). As expected, freshwater is most influential on the surface variables and in particular on horizontal currents, salinity, temperature and surface elevations (Figure 20a).

Tidal forcing seems to have an influence comparable to freshwater. Tides are, however, more influential on the variables below 10 meters (Figure 20b). Tides have

strong effects on the vertical transports, which in turn influence nutrients and biological production.

Effect runs

Non-sinking dissolved particles

Adding non-sinking inorganic particles to river water will increase the light attenuation coefficient of the water. This reduces the amount of light in depth, which will influence the photosynthetic production. Increased inorganic particles in the river water cause a distinct reduction in the phytoplankton biomass (Figure 21). The effect is most pronounced in the diatom biomass (Figure 21). This is not unexpected, since diatoms are located deeper and thus are more susceptible to changes in light attenuation. Reduced consumption of inorganic nutrients and a reduced oxygen production (Figure 21) is the consequence of reduced phytoplankton production.

Changing river nitrogen and phosphorous concentrations

Doubling of nitrogen and phosphorous concentrations in river water has relatively small effects. The most evident change is seen in flagellate biomass (Figure 21), which increases slightly in response to the elevated nitrate and phosphorous levels. Diatoms respond with a small biomass reduction (Figure 21). The response in nitrate and phosphate is small, probably because added nutrients enter flagellate biomass.

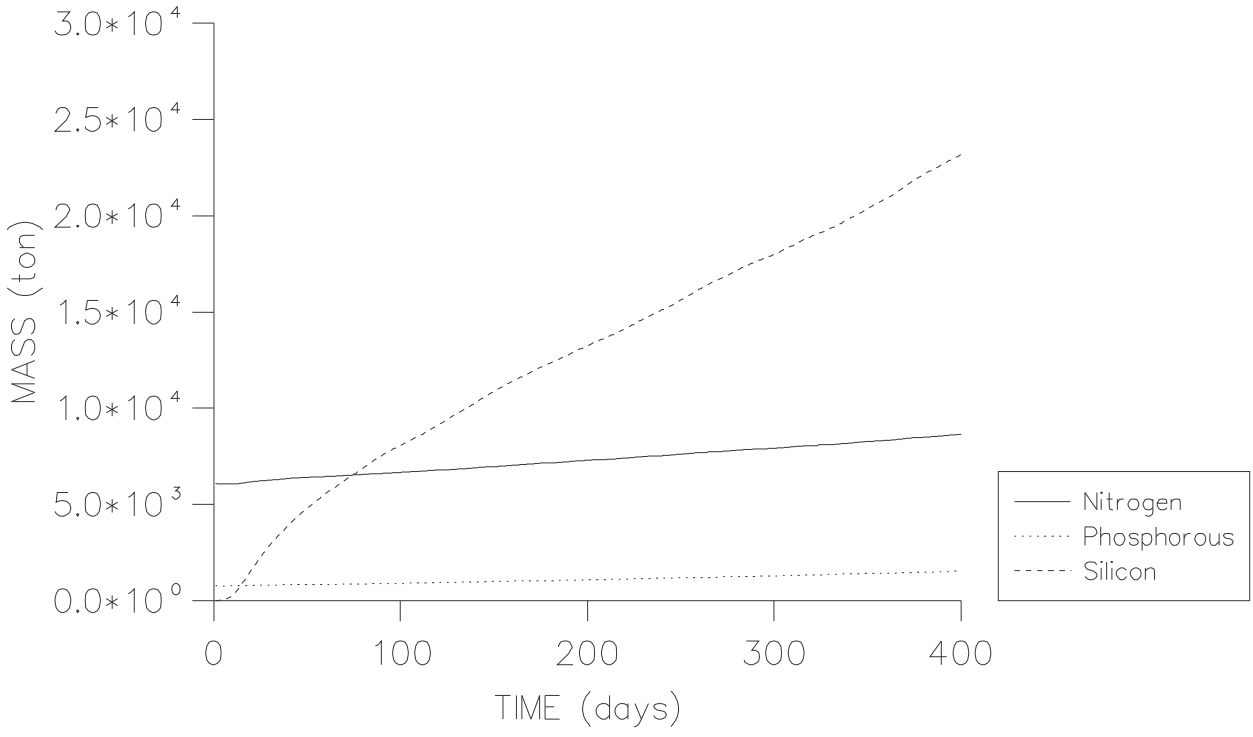

FIGURE 19. Predicted amounts of sediment bound nitrogen, phosphor and silicon in Golfo Dulce.

A

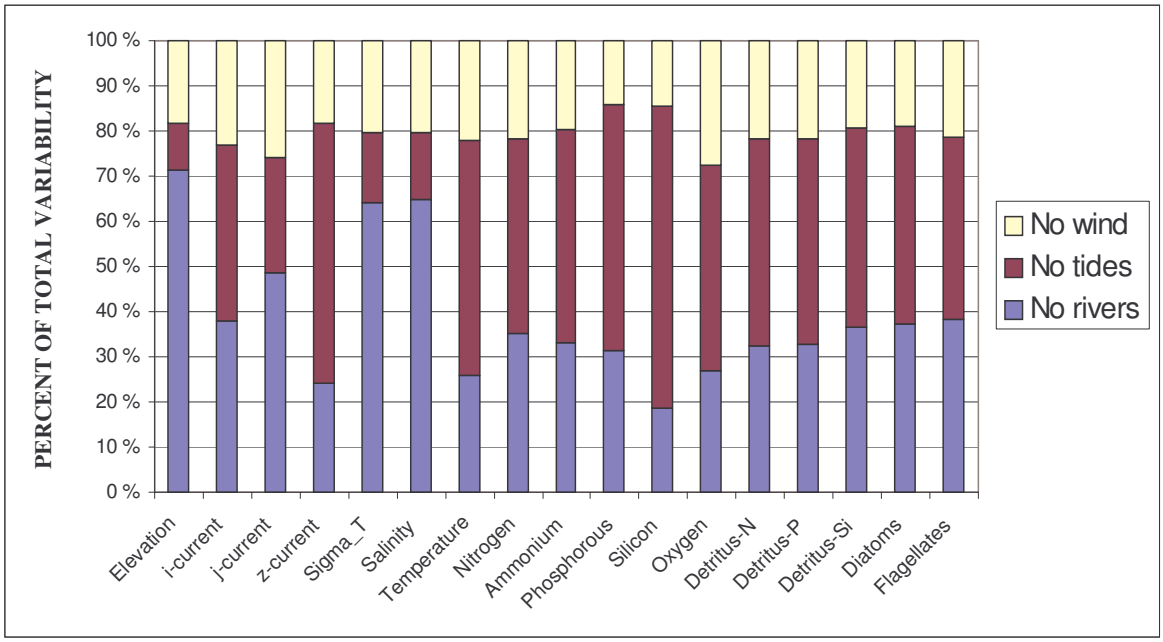

B

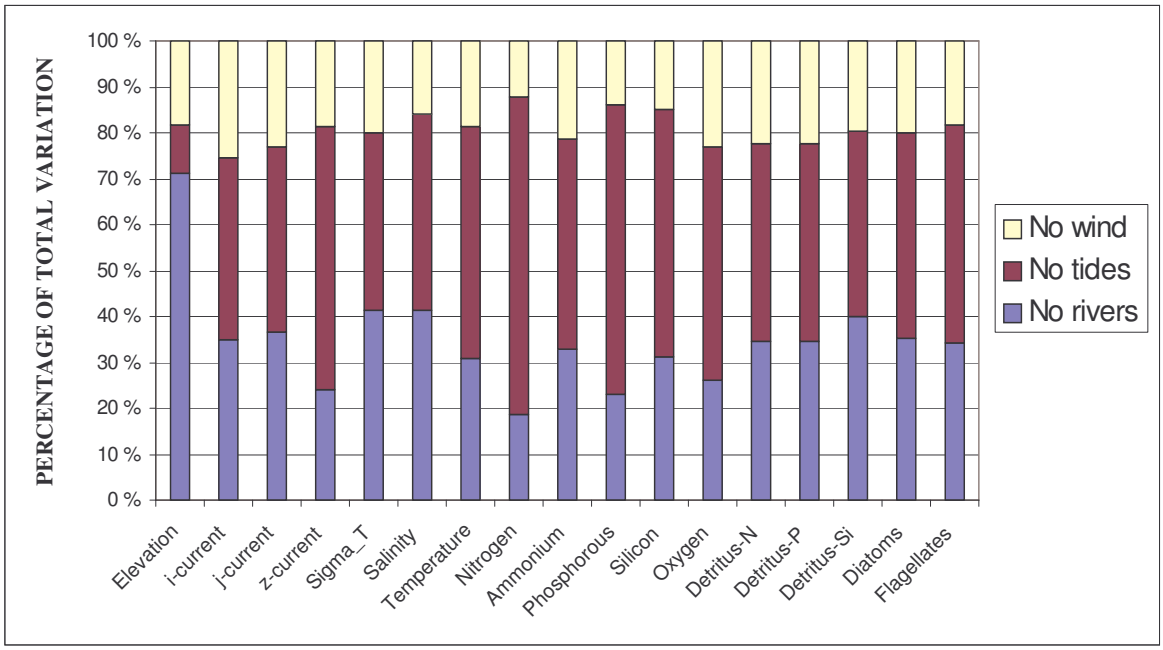

FIGURE 20. Deviations from basic run for some selected variables in simulations with different forcing of wind, rivers and tides. Bars show the relative difference (%) between basic run and simulations where each of the forcing functions are left out. **A)** show the differences at depths above 10 meters **B)** show the differences at depths below 10 meters

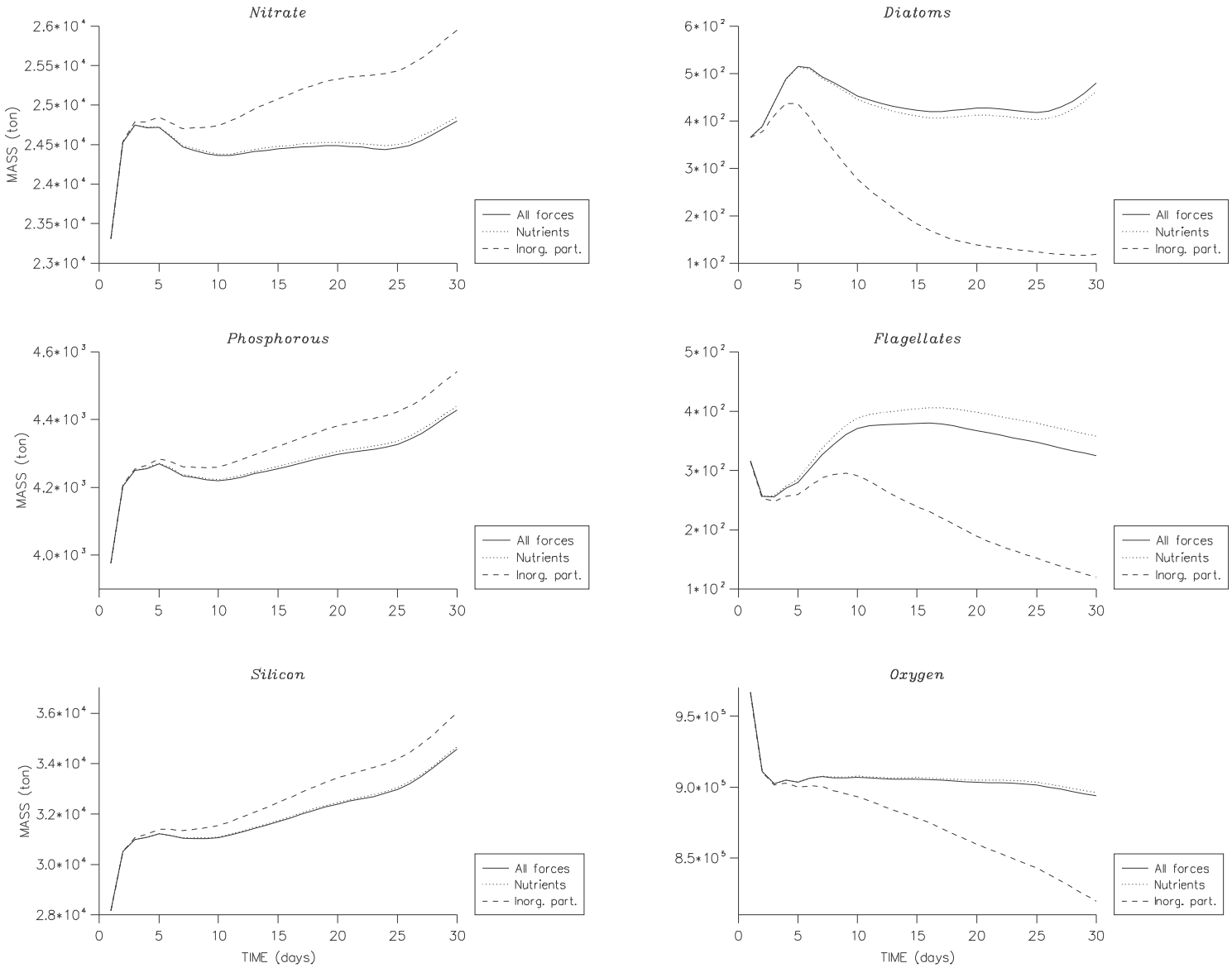

FIGURE 21. Predicted amounts (tons) of nitrogen, phosphorous, silicon, diatoms, flagellates and oxygen during a monthly simulation. The lines show predictions with basic run settings, with doubled concentrations of nitrogen and phosphor in river water and with inorganic substances (20 g m^{-3}) in river water

Discussion

The Coriolis effect has little influence on the predicted circulation, which is not unexpected considering the nearness to equator. Freshwater, wind, tides and bottom topography, on the other hand, all seem to have a significant influence on the predicted circulation in Golfo Dulce. According to previous studies in Golfo Dulce (Quirós 1989, 1990), currents are most pronounced near the sill and in the outer parts of the gulf. The simulations indicate that freshwater is more influential on the circulation than previously assumed (Quirós 1989, 1990). It is important to have in mind the *ad hoc* approach used to estimate river transports (see under "Implementation of the model"). Precipitation is here allocated into four main rivers. In the real system, however, a large part of the precipitation probably enters the gulf via many creeks and smaller rivers (Lizano pers. comm.). This implies that less water would enter via the main rivers. The distribution of water in the rivers is also connected with uncertainty. A different distribution of water in the rivers may affect pressure gradients in the gulf basin, and create different circulation pattern than predicted here. Mixing of river and gulf (fresh and salt) water would also change if less fresh water enter the gulf via large rivers.

The predicted hydrographic variables roughly correspond to observation in the area (Richards et al. 1971; Brenes & Léon 1988; Thamdrup et al. 1996). The model predicts a stratified surface layer, about 50 meter deep, with diluted salinity and temperatures between 24-28 °C. Below this is a homogeneous deep layer with salinity about 34.5 ‰ and temperatures about 23 °C. Predicted temperatures below 50 meters are, in general, higher than observations from the gulf. The initial hydrographic structure and ocean boundary conditions are based on values from the coastal area of Costa Rica (Levitus and Boyer 1994b). The temperatures below 50 meters in these data are generally higher than those observed in Golfo Dulce. Together with freshwater, these data influence the predicted vertical hydrographic structure inside the gulf. Higher water temperatures below sill depth may ease vertical mixing of surface and deeper water, because of reduced density gradients between the water masses.

The use of monthly oceanic wind fields (Oort 1983), with large spatial resolution, may have undermined the true effects from wind on the surface circulation of Golfo Dulce. The rough scaled (in time and space) wind fields do not account for local topography, which may alter both direction and speed of wind. Short time events, such as hurricanes, which may have strong effects on local time scales, are also smoothed out in these data sets.

Predicted vertical profiles of nutrients and oxygen deviate relatively much from observations in the gulf (Richards et al. 1971; Brenes & Léon 1988; Thamdrup et al. 1996). Predicted nitrate distribution increases with depth (Figure 14) in contrast to observed values where the maximum concentrations occur around sill depth (Richards et al. 1971; Brenes & Léon 1988; Thamdrup et al. 1996; Córdoba and Vargas 1996). Richards et al. (1971) explained the decreasing nitrate concentrations below sill depth with denitrification and nitrate reduction processes. Predictions indicate that denitrification rate (Eq. B1.2, Table 4b) may be too low here, and that photosynthetic nitrogen consumption is too low above sill depth.

Modelled phosphate and silicate concentrations (Figure 14) have vertical profiles similar to observations (Richards et al. 1971; Brenes & Léon 1988; Thamdrup et al. 1996, Córdoba and Vargas 1996), although modelled values are about 20 and 8 fold higher for phosphate and silicate, respectively.

The predicted vertical oxygen profiles (Figure 14) are correct, but the concentrations are about 50 fold higher than observed values. The model does not predict anoxic conditions as observed in the deeper inner basin of Golfo Dulce (Richards et al. 1971; Brenes & Léon 1988; Thamdrup et al. 1996, Córdoba and Vargas 1996).

The large deviations between predicted and observed nutrients and oxygen may relate to many factors. Coefficients determining rates and temperature dependencies of processes such as mineralisation, nitrification, denitrification and photosynthesis should be adjusted for tropical conditions. Predicted concentrations also depend on the transports predicted by the physical model. The model predicts an accumulation of N,P and Si nutrients (Figure 15) in Golfo Dulce. Nutrient accumulation is partly a result of outflowing nutrient poor surface water combined with the inflow of deep nutrient rich water. Concentrations of nutrients and organic particles in the coastal water may thus influence the nutrient concentrations inside the gulf. Although the simulations with elevated nutrient levels in rivers had little effect, the river input of nutrients will also contribute to the nutrient enrichment of the gulf.

The model fails to predict anoxic conditions in the deeper layers of Golfo Dulce. Too strong vertical mixing may prevent anoxic conditions in the deeper gulf, since oxygen rich surface water is then mixed into the bottom water. Running the model without the physical transports (only sinking of detritus and diatoms) generates anoxic conditions below the eupothic zone. A possible overrated vertical mixing may be enhanced by weaker temperature gradients. The predicted estuarine circulation may also be overrated because of overestimated river flows. This may increase the turbulent mixing between water above and below sill depth.

There are few data available for evaluation of predicted biological production in Golfo Dulce. Comparing modelled summer phytoplankton biomass (Figure 15) in Golfo Dulce, about 978 g wet weight m^{-2} (C:N = 0.0119 Aksnes & Lie 1990; C:Wet = 12.5 Parsons et al. 1977; ton:g m^{-2} = $1.33 \cdot 10^{-3}$), with values from coastal water in the Costa Rica region, which is about 3.75 g wet weight m^{-2} (Blackburn et al. 1970; Conover et al. 1974; Kuntz et al. 1975), gives a factor of difference about 260. It is not unrealistic that production in Golfo Dulce is higher than in coastal water, because of river inputs, but the large differences is most likely caused by inappropriate parameter settings in the processes determining phytoplankton production. The parameters have the same settings as in the original models (Aksnes et al. 1994, 1995; Savchuk and Wulff 1996; Berntsen et al. 1997) developed for temperate systems. Modelled phytoplankton mortality represents about 10 percent losses each day, which is probably too low for tropical oceans. Higher grazing mortality would not necessarily reduce standing phytoplankton biomass, but it would increase the respiration in the system directly through grazing, and indirectly through increased detritus production and mineralisation of this. Higher grazing rate may shift the oxygen balance and generate anoxic bottom conditions.

Surface light (Appendix) is another crucial variable for phytoplankton production. Light attenuation is calculated from a coefficient for seawater and a function describing attenuation from phytoplankton (Chl. a, see Table A1 in Appendix). Possible underestimates of light attenuation may have resulted in unrealistically high phytoplankton growth potential. Eroded material from land is also a factor with strong influence on light conditions. In the effect runs, dissolved inorganic particles are introduced via rivers (Figure 21). They turned out to have strong negative influence on

the phytoplankton production. The problem with dissolved particles is how to characterise the particles (size, shape), since this will influence the way it affects light attenuation and scattering (Apel 1987). The simulation presented here used data from Vant (1990) to calculate influence from inorganic particles on attenuation. Currently there are no data available on the concentrations of dissolved inorganic substances and particles in the rivers of Golfo Dulce.

River input of nutrients and detritus will also influence phytoplankton production and concentrations of dead organic material in the gulf. Although the results presented here (Figure 21) indicate a relatively weak effect of river nutrients, this must be seen in connection with the low background levels of river nutrients here. An interesting result of changed river nutrients was the small switch in abundance between the phytoplankton groups. River nutrient concentrations are here based on data from Coto and connected rivers (Michels unpubl. data). There is no information on the organic contents in river water entering Golfo Dulce. This factor was, therefore, set to zero in the annual runs.

From the dynamics of nutrients and phytoplankton in the euphotic zone (Figure 15) it seems that available phosphorous and silicon in the euphotic zone limit phytoplankton production. Flagellate production seems limited by phosphorous nutrients, while diatom production seems limited mainly by silicon nutrients. Low silicon concentrations near surface prevent diatom growth, which in turn creates a non-competitive window for the flagellates. Consequently, diatoms are located deeper and near the sill (Figure 16) where silicon rich deeper water is mixed into the surface water, while flagellates are found near the surface (Figure 17) inside the gulf. The distribution of diatoms and flagellates is driven by the freshwater runoff, which creates a brackish surface layer rich in nitrate and phosphate, but low in silicate. The nutrient dynamics inside Golfo Dulce depend on water transports across the sill, and the nutrient concentrations in the exchanged water. These processes also have strong influence on the dynamics of the phytoplankton community in Golfo Dulce.

There are few empirical data available to develop satisfactory forcing functions to the model. This makes it difficult to run realistic simulations or to attempt a validation of the model by comparing predictions and observations. The primary motivation for this report has, therefore, been to document and demonstrate the potential output from the model. Aware of the limitations of the current model settings, the results may give an indication of how the different forcing functions possibly influence the system dynamics. Future work involves the generation of better empirical data (spatial and temporal) to force the physical model, i. e. local wind fields, fresh water runoff, local current patterns and hydrographic structure in the coastal zone near the gulf entrance. The biological model needs better empirical data to generate forcing, i. e. nutrients, organic and inorganic matter in river water and at the ocean boundaries. Although the structure of the biological model may be general, i. e. valid in tropical and temperate localities, it will probably need an upgrade of the parameter settings. Adjusting the parameters of the model should be based on experimental or field based measurements.

Acknowledgements

Thanks to The Research Council of Norway who financed this project. Thanks to the initiator of the project, Professor Ulf Lie, for help and advice during the project. Thanks to Professor Jarle Berntsen, Professor Harald Svendsen and research fellow Lars Asplin for assistance with the physical model, and Professor Dag Aksnes for advises on biological subjects. Finally, thanks to staff at Parallab (University of Bergen) for support during trouble shooting during the computer simulations.

References

Aksnes, D. L., J. K. Egge, R. Rosland & B. Heimdal 1994. Representation of *Emiliania huxleyi* in phytoplankton simulation models. A first approach. *Sarsia* 79: 291-300.

Aksnes, D. L. & U. Lie 1991. A coupled physical-biological pelagic model of a shallow sill fjord. *Estuarine, Coastal and Shelf Science* 31:459-486.

Aksnes, D. L., K. B. Ulvestad, B. M. Baliño, J. Berntsen, J. K. Egge & E. Svendsen 1995. Ecological modelling in coastal waters: towards predictive physical-chemical-biological simulation models. *Ophelia* 41:5-36.

Apel, J. R. 1987. *Principles of ocean physics*. Academic Press, London. 634 p.

Berntsen, J., D. L. Aksnes & A. Foldvik 1997. *Fresh water driven production in a fjord.* Report no. 7, Department of Applied Mathematics, University of Bergen 1997. 43p.

Berntsen, J., M. D. Skogen & T. O. Espelid 1996. Description of a sigma-coordinate ocean model. *Fisken og havet* 12. 33 p.

Berrangé, J. P. 1989. The Osa group: An auriferous pliocene sedimentary unit from the Osa Peninsula, southern Costa Rica. *Rev. Geol. Amer. Centr.* 10:67-93.

Blackburn, M., R. M. Laurs, R. W. Owen & B. Zeitzschel 1970. Seasonal and areal changes in standing stocks of phytoplankton and micronecton in the eastern tropical pacific. *Marine Biology* 7:14-31.

Blumberg, A. F. & G. L. Mellor 1987. A description of a three-dimensional coastal ocean circulation model. -In N. Heaps (ed.): *Three-Dimensional Coastal Ocean Models, Vol. 4*. American Geophysical Union, Washington D. C.

Brenes, C. L. & S. Léon 1988. Algunos aspectos físico-quÍmicos del Golfo Dulce. *Ing. Cienc. Quím.* 12, (1-2):12-16.

Caraco, N. F., J. J. Cole & G. E. Likens 1989. Evidence for sulfate controlled phosphorous release from sediments of aquatic systems. *Nature* 341:316-318.

Caraco, N. F., J. J. Cole & G. E. Likens 1990. A comparison of phosphorous immobilization in sediments of freshwater and coastal marine systems. *Biogeochemistry* 9:277-290.

Conkright, M., S. Levitus & T. Boyer 1994. *World Ocean Atlas 1994 Volume 1: Nutrients*. NOAA Atlas NESDIS 1, U.S. Department of Commerce, Washington, D.C.

Conover, R. J. 1974. Production in marine plankton communities. *Proceedings of the First International Congress of Ecology*, pp. 159-63. Centre for Agricultural Publishing and Documentation, Wageningen, Netherlands.

Córdoba, R. & J. A. Vargas 1996. Temperature, salinity, oxygen, and nutrient profiles at a 200 m deep station in Golfo Dulce, Pacific coast of Costa Rica. *Revista De Biologia Tropical 44* (Supplement 3): 233-236.

Cortés, J. 1990. The coral reefs of Golfo Dulce, Costa Rica: distribution and community structure. *Atoll Research Bulletin* No. 344. 37 p.

Enoksson, V., F. Sorensson & W. Graneli 1990. Nitrogen transformations in the Kattegat. *Ambio* 19:159-166.
Gundersen, K. & C. W. Mountain 1973. Oxygen utilization and PH changes in the ocean resulting from biological nitrate formation. *Deep Sea Research* 20:1083-1091.
Gutierres, A. B. *Unpublished tidal data from station Quepos at the Pacific coast of Costa Rica.*
Hebbeln, D., D. Beese & J. Cortés 1996. Morphology and sediment structure in Golfo Dulce, Costa Rica. *Revista De Biologia Tropical* 44 (Supplement 3):1-10.
Henriksen, K. & W. M. Kemp 1988. Nitrification in marine and coastal marine sediments. In: Blackburn T. H. & J. Sorensen (eds). *Nitrogen cycling in coastal marine environments.* N. Y. Wiley and Sons Ltd.:207-249.
Herrera, W. 1985. *Clima de Costa Rica*. Editorial Universidad Estatial a Distancia, San José, Costa Rica.
Jørgensen, S. E. 1994. *Fundamentals of ecological modelling*. Elsevier, Amsterdam. 628 p.
Kaplan, W. A. 1983. Nitrification. In: Carpenter, E. J. & D. G. Capone (eds). *Nitrogen in the marine environment*. N. Y., Academic Press: 139-190.
Klump, J. V. & C. V. Martens 1983. Benthic nitrogen regeneration. In: Carpenter, E. J. & D. G. Capone (eds). *Nitrogen in the marine environment*. N. Y., Academic Press: 385-457.
Koike, I. & J. Sørensen 1988. Nitrate reduction and denitrification in marine sediments. In: Blackburn T. H. & J. Sørensen (eds). *Nitrogen cycling in coastal marine environments.* N. Y. Wiley and Sons Ltd.:251-273.
Kuntz, D., T. T. Packard, A. H. Devol & J. J. Anderson 1975. *Chemical, physical and biological observations in the vicinity of the Costa Rica dome (January – February, 1973)*. University of Washington, Dep. of Oceanography, Technical report no. 321. 189 p.
Levitus, S. & T. Boyer 1994a. *World Ocean Atlas 1994 Volume 2: Oxygen.* NOAA Atlas NESDIS 2, U.S. Department of Commerce, Washington, D.C.
Levitus, S. & T. Boyer 1994b. *World Ocean Atlas 1994 Volume 4: Temperature.* NOAA Atlas NESDIS 4, U.S. Department of Commerce, Washington, D.C.
Levitus, S., R. Burgett & T. Boyer 1994. *World Ocean Atlas 1994 Volume 3: Nutrients.* NOAA Atlas NESDIS 3, U.S. Department of Commerce, Washington, D.C.
Lohse, L., J. F. P. Malschaert, C. P. Slomp, W. Helder & W. van Raaphorst 1993. Nitrogen cycling in North Sea sediments: interactions of denitrification and nitrification in offshore and coastal areas. *Marine Ecology Progress Series* 101:283-296.
Michels, A. *Unpublished data on nutrients and temperatures from the river Coto and associated river systems.*
Martinsen, E. A. & H. Engedahl 1987. Implementation and testing of a lateral boundary scheme as an open boundary condition in a barotropic ocean model. *Coastal Engineering* 11:603-627.
Mellor, G. L. & T. Yamada 1982. Development of a turbulence closure model for geophysical fluid problems. *Reviews of geophysics and space physics* 20:851-875.
Oort, A. 1983. *Global atmospheric circulation statistics, 1958-1973*. NOAA Professional Paper 14, U.S. Department of Commerce, Washington, D.C.
Parsons, T. R., M. Takahashi & B. Hargrave 1977. *Biological oceanographic processes. 2nd ed.* Pergamon. New York. 332 p.
Quirós, G. E. 1989. *Corrientes residuales en Golfo Dulce*. Informe Técnico, SeccÛn Oceanografia, Departemento de Fisica, Universidad Nacional, Heredia, Costa Rica. 27 pp.

Quirós, G. E. 1990. *Establicemento de una finca productora de camarones en el alto Golfo Dulce*. Informacíon técnica fundamental, climatología, oceanografía, ecología. Manuscript. Secciún de Oceanografía, Departemento de Fisica, Universidad Nacional, Heredia, Costa Rica. 17 p.

Richards, F. A., J. J. Anderson & J. D. Cline 1971. Chemical and physical observations in Golfo Dulce, an anoxic basin on the Pacific coast of Costa Rica. *Limnology and Oceanography* 16:43-50.

Sader, S. A. & A. T. Joyce 1988. Deforestation rates and trends in Costa Rica, 1940 to 1983. *Biotropica* 20:11-19.

Santschi, P., P. Hohener, G. Benoit & M. Buchholtz-ten Brink 1990. Chemical processes at the sediment-water interface. *Marine Chemistry* 30:269-315.

Savchuk, O, & F. Wulff 1996. *Biogeochemical transformations of nitrogen and phosphorus in the marine environment -- coupling hydrodynamic and biogeochemical processes in models for the Baltic Proper*. Syst. Ecol. Contrib. Stockholm-Sweden Vol. 2, 79 pp.

Seitzinger, S. P. 1988. Denitrification in freshwater and coastal ecosystems: ecological and geochemical significance. *Limnology and Oceanography* 33:702-724.

Seitzinger, S. P., W. S. Gardner & A. K. Spratt 1991. The effect of salinity on ammonium sorption in aquatic sediments: implementations for benthic nutrient recycling. *Estuaries* 14:167-174.

Stephens, D. W. & J. R. Krebs (1986). *Foraging theory*. Princeton University Press NJ. 247 p.

Skogen, M. D., E. Svendsen, J. Berntsen, D. Aksnes & K. B. Ulvestad 1995. Modelling the primary production in the North Sea using a coupled three-dimensional physical-chemical-biological ocean model. *Estuarine, Coastal and Shelf Science* 41:545-565.

Sundby, B., C. Gobeil, N. Silverberg & A. Mucci 1992. The ephosphorous cycle in coastal marine sediments. *Limnology and Oceanography* 37:1129-1145.

Thamdrup, Bo, D. E. Canfield, T. G. Ferdelman, R. N. Glud & J. Gundersen 1996. A biochemical survey of the anoxic basin Golfo Dulce, Costa Rica. *Revista De Biologia Tropical* 44 (Supplement 3):19-33.

Vant, W. N. 1990. Causes of light attenuation in nine New Zealand Estuaries. *Estuarine, Coastal and Shelf Science* 31:125-137.

Visser, A. W. & L. Kamp-Nielsen 1996. The use of models in eutrophication studies. Pp. 221-242 in: Bo Barker Jørgesen & Katherine Richardson (eds). *Eutrophication in coastal marine ecosystems*. American Geophysical Union. Washington D.C. 272 p.

Wolff, M., H. J. Hartmann & V. Koch 1996. A pilot trophic model for Golfo Dulce, a fjord-like tropical embayment, Costa Rica. *Revista de Biologica Tropical* 44 (Supplement 3) 44:215-231.

Wolff, M. & J. A. Vargas (eds) 1994. *RV Victor Hensen expedition 1993/1994* - Cruise report. ZMT contribution no. 2, 109 p.

Yukihira, H. 1991 *Algunos par·metros del ambiente acu·tico de la Bahía Golfito y el Golfo Dulce relacionados con su potencial para el culvito de moluscos*. Manuscipt, Esc. de Scientas Biologicas, Universidad de Nacional, Heredia, Costa Rica/Servicio de Voluntarios Japoneses (JOCV/JICA). 23 p.

Appendix 1: Model for surface radiation and light in depth

Surface light is here calculated from a model for solar radiation developed by Skartveit & Olseth (1986, 1988). The parameters and variables of the radiation model is listed in Tables A1 and A2, respectively. Sun declination (δ) is given as a function of day number (n):

$$\sin(\delta) = 0.3979\sin(0.9856(n-80) + 1.917[\sin(0.9856n) - 0.98112]) \quad \text{R1}$$

CET represents Norwegian normal time and *L* the longitude. According to Skartveit & Olseth (1988) the real sun time (*SST*) may then be expressed as:

$$SST = CET + (L-15) - 0.4083\sin[0.9856(n-80)] - 1.7958\cos[0.9856(n-80)] + 2.4875\sin[1.9712(n-80)] \quad \text{R2}$$

and the sun elevation (h) may then be computed from:

$$\sin(h) = \sin(\delta)\sin(B) - \cos(\delta)\cos(B)\cos(SST) \quad \text{R3}$$

where *B* represents the latitude.

Incident radiation is modeled from a formulation where mean irradiation is a function of latitude and season. Mean climatological irradiance varies according to a presumed sinusoidal variation and all constants, a_x - f_x (Table A1), should ideally be specific for the object area. In lack of data on these parameters for Costa Rica the model is run with the values obtained for Bergen. Irradiance is split into diffuse (x = *dif*) and direct (x=*dir*), or beam, components:

$$H_x(h,n) = I_0(n) \cdot Tr_{0x}(n) \cdot F_x(h) \quad \text{R4}$$

$H_x(h,n)$ represents direct or diffuse irradiance at the surface, $I_o(n)$ the solar irradiance at normal incidence just outside the atmosphere, $Tr_{ox}(n)$ the transmittance and $F_x(h)$ the solar elevation function. Transmittance at overhead zenith sun is given by:

$$Tr_{0x}(n) = a_x\left[1 + b_x\cos\left(\frac{n-c_x}{365}2\pi\right)\right] \quad \text{R5}$$

The solar elevation function $F_x(h)$ express the effect of varying solar elevation (h) and is given by:

$$F_x(h) = 1 - d_x + e_x + d_x\sin(h) - e_x[\sin(h)]^{0.5} \quad \text{R6}$$

The formulas are valid only for sun elevations above 5 degrees and solar radiation is set to zero for elevations below 5 degrees. The function for solar irradiance is:

$$I_0(n) = 1367 \cdot (1 + 0.003346\cos[0.9856(n-3)]) \quad \text{R7}$$

Following the procedure above we may now approximate the incident direct and diffuse irradiation at the surface. In our model we need, however, the photosynthetic active irradiation at different depths of the water column. The diffuse light is calculated from:

$$I_{dif}(x,y,z,t) = PAR \cdot R_{dif}(x,y,t) \cdot e^{-\frac{\kappa(x,y,z,t)}{\mu}} \qquad \text{R8}$$

where $R_{dif}(x,y,t) = H_{dif}(h,n)$, the diffuse component of the surface irradiance, and *PAR*, photosynthetic available radiance, a constant which converts from incident diffuse irradiation to photosynthetic active irradiation. μ is the mean cosine of the diffuse light and κ is the attenuation coefficient which is kept as a function of the concentration of chlorophyll and other substances:

$$\kappa = b_1 z + \int_z^0 \left(b_2 \cdot E(x,y,z,t) + b_3 \cdot \left[Dia(x,y,z,t) + Fla(x,y,z,t) \right] \right) dz \qquad \text{R9}$$

References

Skartveit, A. & J. A. Olseth 1986. Modelling slope irradiance at high latitudes. *Solar Energy* 36:333-344.

Skartveit, A. & J. A. Olseth 1988. *Varighets tabeller for timevis belysning mot 5 flater pÂ 16 norske stasjoner*. Technical Report Rapport 7-1988. Geophysical institute, Meteorological Division, Allegt. 70, N-5007 Bergen, Norway.

Table A1. Parameters in the radiation model

SYMBOL	DESCRIPTION	VALUE/UNIT
a_{dif}	coefficient for diffuse radiation	0.094
a_{dir}	coefficient for direct radiation	0.722
b_{dif}	coefficient for diffuse radiation	0.052
b_{dir}	coefficient for direct radiation	0.044
c_{dif}	coefficient for diffuse radiation	64
c_{dir}	coefficient for direct radiation	21
d_{dif}	coefficient for diffuse radiation	-0.432
d_{dir}	coefficient for direct radiation	1.643
e_{dif}	coefficient for diffuse radiation	1.718
e_{dir}	coefficient for direct radiation	-0.748
μ	mean cosine of diffuse light	0.83
b_1	extinction due to water	0.07 m^{-1}
b_2	extinction due to inorganic substances	0.1 m^{-1}
b_3	extinction due to algae	$1.25 \cdot 10^{-3}$ m $(mgN)^{-1}$
PAR	photosyntetic active radiation	0.40

Table A2. Variables in the radiation model

SYMBOL	DESCRIPTION	VALUE/UNIT
B	latitude	radians
CET	Norwegian normal time	-
δ	sun declination	radians
F_x	solar elevation function	radians
h	sun elevation	radians
H_x	surface irradiance (diffuse/direct)	uE m^{-2} s^{-1}
i	grid horizontal location index	-
I_0	solar irradiance outside atmosphere	uE m^{-2} s^{-1}
j	grid horizontal location index	-
κ	attenuation coefficient	m^{-1}
n	Julian day number	1-365
SST	real sun time	-
Tr_{0x}	transmittance	-
x	refers to direct and diffuse irradiance	1.34
z	grid vertical location index	-

Appendix 2. Forcing data at the ocean boundary and rivers

Ocean boundary forcing: salinity and temperature

Abbreviations and units: M=month, D=depth (m), S=salinity(‰), T=temperature(°C)

M	D	S	T	M	D	S	T
1	0	31.24	28,22	4	250	34.89	
1	10	31.76	28,17	4	300	34.81	
1	20	32.46	27,86	4	400	34.76	
1	30	33.10	26,83	4	500	34.70	
1	50	34.21	22,10	4	600	34.66	
1	75	34.85		4	700	34.63	
1	100	34.94		4	800	34.60	
1	125	34.97		4	900	34.60	
1	150	34.96		4	1000	34.61	10,00
1	200	34.93		5	0	32.90	28,83
1	250	34.90		5	10	33.16	28,57
1	300	34.84		5	20	33.64	27,42
1	400	34.72		5	30	34.04	24,97
1	500	34.64		5	50	34.57	20,69
1	600	34.61		5	75	34.87	
1	700	34.58		5	100	34.97	
1	800	34.58		5	125	35.00	
1	900	34.60		5	150	34.96	
1	1000	34.58	10,00	5	200	34.89	
2	0	31.92	28,11	5	250	34.85	
2	10	32.23	27,88	5	300	34.80	
2	20	32.92	26,94	5	400	34.70	
2	30	33.81	25,27	5	500	34.65	
2	50	34.58	20,76	5	600	34.59	
2	75	34.90		5	700	34.59	
2	100	34.96		5	800	34.58	
2	125	34.99		5	900	34.60	
2	150	34.97		5	1000	34.58	10,00
2	200	34.93		6	0	32.74	28,34
2	250	34.87		6	10	33.12	28,15
2	300	34.81		6	20	33.69	27,39
2	400	34.69		6	30	34.08	25,35
2	500	34.64		6	50	34.78	20,94
2	600	34.60		6	75	35.06	
2	700	34.59		6	100	35.13	
2	800	34.60		6	125	35.16	
2	900	34.60		6	150	35.15	
2	1000	34.60	10,00	6	200	34.87	
3	0	31.74	28,40	6	250	34.92	
3	10	31.98	28,10	6	300	34.88	
3	20	32.76	26,95	6	400	34.78	
3	30	33.50	24,99	6	500	34.67	
3	50	34.46	20,38	6	600	34.57	
3	75	34.86		6	700	34.60	
3	100	34.95		6	800	34.58	
3	125	34.99		6	900	34.61	
3	150	34.97		6	1000	34.59	10,00
3	200	34.91		7	0	31.40	28,19
3	250	34.88		7	10	31.72	28,14
3	300	34.82		7	20	32.74	27,71
3	400	34.71		7	30	33.53	25,80
3	500	34.64		7	50	34.64	21,45
3	600	34.64		7	75	34.90	
3	700	34.59		7	100	34.99	
3	800	34.60		7	125	35.03	
3	900	34.59		7	150	35.01	
3	1000	34.57	10,00	7	200	34.95	
4	0	32.51	28,74	7	250	34.93	
4	10	33.19	28,24	7	300	34.82	
4	20	33.96	26,35	7	400	34.71	
4	30	34.33	23,76	7	500	34.65	
4	50	34.71	19,82	7	600	34.60	
4	75	34.96		7	700	34.58	
4	100	35.01		7	800	34.58	
4	125	35.04		7	900	34.58	
4	150	35.01		7	1000	34.57	10,00
4	200	34.92					

M	D	S	T
8	0	32.18	27,92
8	10	32.46	27,82
8	20	32.86	27,19
8	30	33.83	25,04
8	50	34.61	20,42
8	75	34.86	
8	100	34.94	
8	125	34.97	
8	150	34.97	
8	200	34.91	
8	250	34.88	
8	300	34.82	
8	400	34.71	
8	500	34.65	
8	600	34.60	
8	700	34.58	
8	800	34.59	
8	900	34.59	
8	1000	34.58	10,00
9	0	31.16	27,92
9	10	31.85	27,84
9	20	32.18	27,25
9	30	33.15	24,97
9	50	34.59	20,08
9	75	34.90	
9	100	34.98	
9	125	34.99	
9	150	34.97	
9	200	34.91	
9	250	34.87	
9	300	34.81	
9	400	34.70	
9	500	34.64	
9	600	34.62	
9	700	34.61	
9	800	34.59	
9	900	34.56	
9	1000	34.56	10,00
10	0	31.69	27,55
10	10	31.69	27,52
10	20	32.30	27,29
10	30	33.04	25,80
10	50	34.31	21,04
10	75	34.88	
10	100	34.94	
10	125	34.97	
10	150	34.96	
10	200	34.93	
10	250	34.89	
10	300	34.83	
10	400	34.71	
10	500	34.63	
10	600	34.58	
10	700	34.57	
10	800	34.56	
10	900	34.57	
10	1000	34.59	10,00
11	0	31.87	27,25
11	10	32.06	27,17
11	20	32.67	26,97
11	30	33.24	25,88
11	50	34.28	21,26
11	75	34.85	
11	100	34.92	
11	125	34.94	
11	150	34.93	
11	200	34.89	
11	250	34.85	
11	300	34.78	
11	400	34.67	
11	500	34.61	
11	600	34.59	
11	700	34.56	
11	800	34.55	
11	900	34.57	
11	1000	34.56	10,00
12	0	31.26	27,88
12	10	31.45	27,81
12	20	31.83	27,65
12	30	32.44	26,74
12	50	33.87	22,71
12	75	34.72	
12	100	34.93	
12	125	34.95	
12	150	34.97	
12	200	34.94	
12	250	34.91	
12	300	34.89	
12	400	34.72	
12	500	34.58	
12	600	34.61	
12	700	34.58	
12	800	34.57	
12	900	34.58	
12	1000	34.54	10,00

Ocean boundary forcing: nutrients and oxygen

Units: depth (m), nutrients (mg m^{-3}), oxygen (g m^{-3})

Depth	NO_3	PO_4	SiO_4	O_2
0	6.9938	9.4939	108.3319	6.7371
10	18.4645	11.5967	117.3418	6.6608
20	47.1275	16.0301	120.7954	6.2361
30	113.3304	23.2461	153.2169	5.4763
50	249.0271	40.5645	297.6669	3.3461
75	343.6765	52.6165	452.7406	1.8858
100	380.7428	57.9402	530.2915	1.5522
125	402.1479	61.0419	574.0655	1.3709
150	421.2961	62.3875	606.2974	1.2791
200	442.1997	67.3427	675.4535	1.0369
250	455.7362	73.0319	778.3387	0.7624
300	465.7323	77.5164	905.3604	0.5823
400	505.2209	87.0923	1170.3643	0.4202
500	554.1788	92.4966	1512.4695	0.4627
600	595.3241	98.2167	1756.7290	0.2971
700	613.3130	103.2710	2031.0476	0.5955
800	613.3655	95.8707	2124.0508	1.0077
900	579.1671	97.3681	2503.0142	1.2477
1000	613.9609	100.0176	2715.5840	1.5017

River water

Temperature and nutrient contents

T 26.72 (°C)
NO_3 85.00 (mg m^{-3})
NH_4 0.00 (mg m^{-3})
PO_4 15.20 (mg m^{-3})
SiO_4 12.86 (mg m^{-3})